Application of cobalt complexes containing SNS ligands as catalysts for biomimetic paraffin activation

by

Lynette Komarsamy

Dissertation submitted in fulfilment of the academic requirements for the degree of Master of Science in the School of Chemistry & Physics, University of KwaZulu-Natal, Durban, South Africa

As the candidate's supervisors we have approved this dissertation for submission.

Signed _____ Name _____ Date _____

Signed _____ Name _____ Date _____

February, 2012

Abstract

A series of SNS ligands have been successfully synthesised and characterised by IR, NMR and MS. The ligands are divided into two groups and represented by the general formulae: 2,6-bis($RSCH_2$)pyridine [R= methyl, ethyl, butyl, cyclohexyl, phenyl] and bis($RSCH_2CH_2$)amine [R= ethyl, butyl, decyl]. Cobalt complexes of the respective ligands with the general formulae Co[2,6-bis($RSCH_2$)pyridine]Cl_2 and Co[bis($RSCH_2CH_2$)amine]Cl_2 were synthesised and characterised by IR, elemental analysis and X-ray crystallography (for selected complexes). Thus, to investigate the electronic and steric effects of the ligand structure on the chemistry and reactivity of the complexes, the substituents bonded to the two sulfur donor atoms were sequentially varied and two different nitrogen sources were chosen. Crystal structures of Co[2,6-bis(CH_2SCH_2)pyridine]Cl_2 (**Ia**), Co[2,6-bis($CH_2CH_2SCH_2$) pyridine]Cl_2 (**IIa**) and Co[2,6-bis($CH_2CH_2CH_2CH_2SCH_2$)pyridine]Cl_2 (**IIIa**) were obtained. It was found that complex **Ia** exists as a molecular dimer linked through two chloride bridges resulting in an octahedral geometry around each metal centre, while complexes **IIa** and **IIIa** are monomers exhibiting a trigonal bypyrimidal geometry. The complexes were tested as catalysts for the activation of paraffinic C−H bonds towards the formation of oxygenated products: octanol, octanone, octanal and octanoic acid from the substrate *n*-octane. Gas chromatography was utilised to quantify the products formed and also to calculate the conversion and selectivity of each catalyst system. The catalytic testing revealed that the ketone products were the most dominant with selectivities of ca. 90%. The catalyst that was the most active was Co[bis($CH_2CH_2SCH_2CH_2$)amine]Cl_2 (**Ib**) with a total *n*-octane conversion of 23%.

Preface

The experimental work described in this thesis was performed in the School of Chemistry, University of KwaZulu-Natal, Durban, from February 2010 to December 2011, under the supervision of Dr M. D. Bala and Prof. H. B. Friedrich.

These studies represent original work by the author and have not otherwise been submitted in any form for any degree or diploma to any tertiary institution. The work of others that has been used in this study is duly acknowledged in the text.

Signed _____ Date _____

Lynette Komarsamy

Declaration 1

Plagiarism

I, ... hereby declare that:

1. The research reported in this thesis, except where otherwise indicated, is my original research.

2. This thesis has not been submitted for any degree or examination at any other university.

3. This thesis does not contain other person's data, pictures, graphs or other information, unless specifically acknowledged as being sourced from other persons.

4. This thesis does not contain other person's writing, unless specifically acknowledged as being sourced from other researchers. Where other written sources have been quoted, then:

    a. Their words have been re-written but the general information attributed to them has been referenced

    b. Where their exact words have been used, then their writing has been placed in italics and inside quotation marks, and referenced.

5. This thesis does not contain text, graphics or tables copied and pasted from the Internet, unless specifically acknowledged, and the source being detailed in the thesis and in the References sections.

Signed _____ Date _____

Lynette Komarsamy

Declaration 2

Scientific Contributions

Publication

Komarsamy, L.; Bala, M. D.; Friedrich, H. B.; Omondi, B. *Acta Crystallographica* **2011**, *E67*, 302.

Conferences

1. Poster titled "Biomimetic paraffin activation studies of Fe-based complexes containing SNS ligand systems", Lynette Komarsamy, Muhammad D. Bala, Holger B. Friedrich, presented at the SACI conference, University of Witwatersrand, Johannesburg, January 2011.

2. Poster titled "Biomimetic paraffin activation studies of Fe-based complexes containing SNS ligand systems", Lynette Komarsamy, Muhammad D. Bala, Holger B. Friedrich, presented at the SACI postgraduate symposium, University of KwaZulu-Natal, Durban, August 2011.

3. Poster titled "Synthesis and characterization of Co complexes containing SNS ligands for application in biomimetic paraffin activation studies", Lynette Komarsamy, Muhammad D. Bala, Holger B. Friedrich, presented at the CATSA conference, Gauteng, December 2011.

Signed _____ Date _____

Lynette Komarsamy

Table of contents

List of figures

List of tables

List of schemes

List of abbreviations

ATR	-	Attenuated total reflectance
but	-	Butyl
CIF	-	Crystallographic information file
cy	-	Cyclohexyl
CYPs	-	Cytochrome P450 monooxygenases
d	-	Doublet
DEPT	-	Distortionless enhancement by polarisation transfer
DCM	-	Dichloromethane
dec	-	Decyl
ESI	-	Electron spray ionisation
et	-	Ethyl
GC	-	Gas chromatography
IR	-	Infrared
L	-	Ligand
M	-	Metal
m	-	Multiplet
me	-	Methyl
MHz	-	Mega Hertz
MMO	-	Methane monooxygenase
mp	-	Melting point
N/A	-	Not applicable
NAD(P)H	-	Nicotinamide adenine dinucleotide phosphate
neg	-	Negative

NMR	-	Nuclear magnetic resonance
ORTEP	-	Oak ridge thermal ellipsoid plot
ph	-	Phenyl
PMT	-	2,6-Pyridine-dimethylene-ditosylate
pos	-	Positive
py	-	Pyridine
RBF	-	Round bottom flask
s	-	Singlet
t	-	Triplet
t-BuOOH	-	*tert*-Butyl hydroperoxide
THF	-	Tetrahydrofuran
TOF	-	Time of flight
TON	-	Turnover number
VCS	-	Vacant coordination site
q	-	Quartet

Acknowledgements

- I gratefully thank c* change and NRF for financial support.
- I would like to acknowledge my supervisor Dr M. D. Bala and my co-supervisor Prof. H. B. Friedrich for their constant guidance and advice.
- I also thank Dr M. Fernandes and Dr B. Omondi for X-ray crystallographic data collection and refinement.
- My extended appreciation goes out to the technical staff at the School of Chemistry: Mrs Anita Naidoo, Mr Dilip Jagjivan, Mr Gregory Moodley, Mr Raj Somaru and Mrs Malini Padayachee.
- I am also grateful to Mrs Charmaine Magwaza and Mrs Jayambal Govender for their efficient assistance with the handling of my orders.
- Special thanks to my lab mates and friends: Mr M. N. Pillay, Ms V. Dukhi, Ms M. Reddy, Ms D. Naicker, Mr E. Kadwa, Mr M. Fadlalla, Ms T. Chetty, Mr L. Chetty, Mr M. N. Cele, and Dr P. Pansuriya for their help, encouragement and support.
- I am forever grateful to my family, friends and pastors for their prayers and support.
- I would like to especially thank my fiancé Jerome for being my pillar of strength and holding my hand through every difficult time.
- Most importantly I would like to honour my Lord and Saviour Jesus Christ for bringing me this far, for without Him I would not be where I am today.

Dedication

This thesis is dedicated to my late mom, Rageni Komarsamy.

CHAPTER ONE

Introduction

1.1 Biomimetic catalysis

The concept of biomimetic catalysis refers to the application of synthetic strategies that imitate the catalytic activity of enzymes.[1] Enzymes are natural catalysts, the incredible activity and selectivity of which offer inspiration to many areas of scientific research that are termed biomimetic. More importantly these biological catalysts have impacted the chemical industry to a great extent. Biological catalysts generally function at ambient conditions and are known to be the most efficient catalytic systems available. Substrates bind to the active site of the enzyme and catalysis is achieved by the action of two or more functional groups that interact with the active site.[1] Binding of the substrate may be accomplished via hydrophobic interaction, metal coordination or Lewis acid-base coordination in aqueous solution, while in non-aqueous solvents, apart from the two latter ways, binding may also occur via ion pairing or hydrogen bonding.[1]

Biomimetic catalysis is becoming increasingly popular as enzymes continue to inspire new methodologies that result in the development and commercialisation of synthetic catalysts. Synthetic catalytic systems generally operate under relatively harsher conditions in order to produce conversions and selectivities that are satisfactory at industrial scales and this has encouraged the developments in alternative methods based on the biomimetic approach, resulting in the use of synthetic catalysts functioning at milder reaction conditions. With much consideration, various commercial catalysts have been developed which are able to follow similar catalytic pathways compared to their natural counterparts. Studies carried out by Leak and Dalton, as cited by Burrington, have shown that enzymes such as hydroxylase can convert paraffins to alcohols with up to 100% selectivity.[2] To date, there is no commercial analogue able to reproduce this remarkable activity, however several catalytic processes have already been established that generate satisfactory results.

1.1.1 Monooxygenases

Monooxygenases are a class of oxidation enzymes that are found in nature. These enzymes are responsible for catalysing the incorporation of a single oxygen atom from molecular oxygen into an organic substrate.[3] The catalytic reaction involves the activation of molecular oxygen (O_2) by the transfer of electrons followed by oxygenation of the substrate.[3] Nature provides a variety of different monooxygenases that are essential in metabolic processes of both eukaryotes and prokaryotes. Two of these monooxgenases relevant to this study are further elaborated below.

1.1.1.1 Cytochrome P450 monooxygenases

One of the main types of monooxygenases is the heme-containing cytochrome P450 monooxygenases (CYPs) found predominantly in eukaryotes i.e. mammals, plants and fungi, however bacteria also contain a range of these enzymes.[3] There exists a variety of different types of CYPs that each serves a specific niche role, however the overall outlook of these enzymes is discussed in general. CYPs are involved in the conversion of relatively inert compounds into more reactive chemicals as well as reducing the toxicity of certain compounds[4] in a series of biological processes. One of the roles that CYPs play is in the biosynthesis of progesterone, by oxidising the aliphatic side chain on cholesterol.[5] CYPs have proven to be highly selective catalysts for the oxidation of organic substrates like alkanes under mild conditions.

The mechanism that was proposed for the hydroxylation of alkanes is represented in Scheme 1.1 which shows the active metal iron centre and the pathways that are followed to achieve the hydroxyl product. The Fe^{II} species binds O_2 which generates a $Fe^{III}-OO\bullet$ intermediate that leads to the formation of $Fe^{III}-OOH$ from the transfer of an electron and a proton to the active site. The $Fe^{IV}=O$ species is then produced which directly oxidises the substrate to yield the hydroxyl or alcohol product with the Fe^{II} centre regenerated. [4,5] The Fe^{III} centre can also be transformed to the high valent Fe^{IV} species via a peroxide shunt.

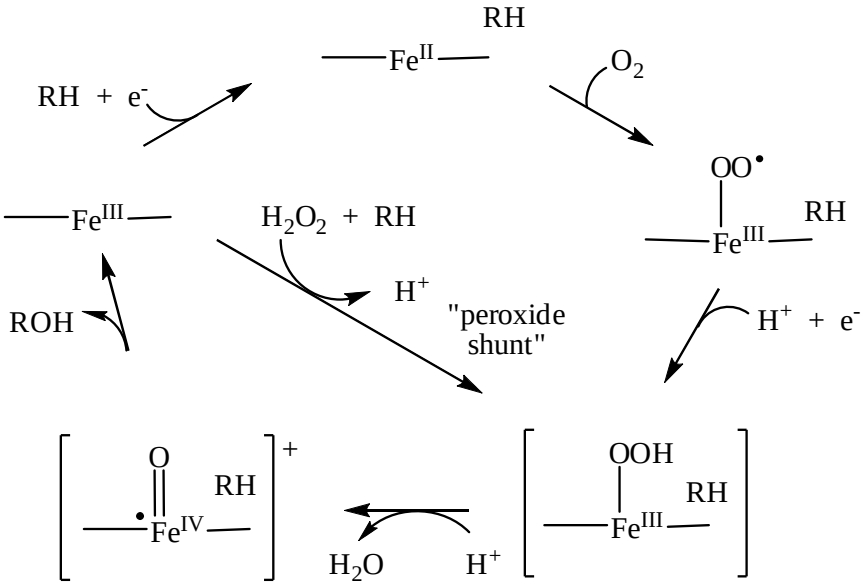

Scheme 1.1: A proposed alkane hydroxylation reaction mechanism for cytochrome P450.[5]

1.1.1.2 Methane monooxygenases

Microorganisms such as methanotrophs contain an enzyme called methane monooxygenase (MMO) which converts methane into methanol during metabolism.[5] In contrast to CYPs, the active site of MMO (Fig. 1.1) has a non-heme, carboxylate-rich diiron structure[5,6] which is responsible for the catalysis. MMO is an enzyme that it not limited to a specific substrate but rather is able to catalyse reactions containing a diverse range of substrates including carbohydrates.[7]

A pathway that is analogous to that of CYPs is observed for MMO with the difference being that all the intermediates are diiron species. The reaction mechanism is initiated by the splitting of the O−O bond of O_2 by two reducing equivalents of the coenzyme nicotinamide adenine dinucleotide phosphate or NAD(P)H. One of the oxygen atoms is reduced to form water as the only by-product while the other oxygen atom is utilised for the oxygenation of the substrate to produce the alcohol product.[7]

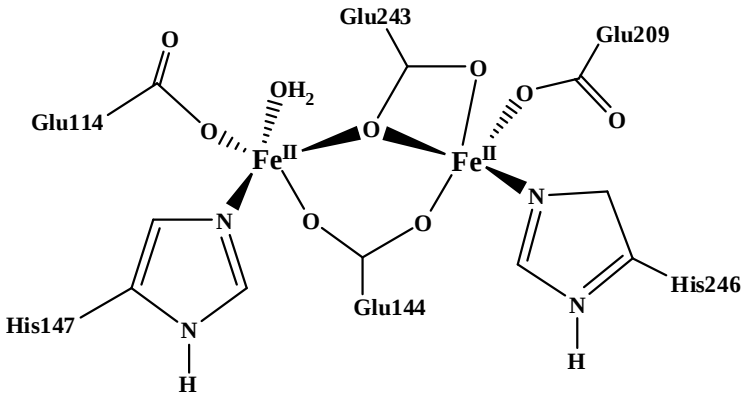

Figure 1.1: Structure of the active site of methane monooxygenase obtained from *Methylococcus capsulatus*.

1.2 Activation and functionalisation of paraffins

Paraffins, generally referring to straight chain alkanes or saturated hydrocarbons, form major components of crude oil and natural gas.[8] Due to the relatively inert nature of the C−H bond, a great deal of research has been done in the area of activation and functionalisation of these unreactive compounds. Their inertness arises from strong, localised C−C and C−H bonds thereby making it difficult for the molecules to participate in a chemical reaction due to the lack of empty orbitals of low energy or filled orbitals of high energy.[8]

Most often paraffins are exploited for energy production in combustion reactions. Hydrocarbons are able to react at high temperatures but these reactions are uncontrollable and usually unwanted products like carbon dioxide and water are formed. For this reason processes have been, and are continually being designed to activate, as well as functionalise, these paraffins in order to convert them into more valuable products that would have wider applications at industrial level. The most common target products are oxygenates, such as alcohols, carboxylic acids, aldehydes and ketones and the process is known as paraffin oxidation. One of the ways of carrying this out is via catalytic systems where a catalyst of interest is utilized to aid in the activation and functionalisation of the paraffin.

As mentioned previously, biological catalysts like hydroxylases are able to perform the conversion of alkanes to alcohols with up to 100% selectivity. These and other biological catalysts, such as the various monooxygenases, have offered inspiration for the development of commercial analogues that are able to catalyse the activation of C−H bonds of

hydrocarbons and subsequently convert them into value-added products that are of higher economic value to industry and greater scientific value to academia.

The term “activation” refers to the C−H bond of the paraffin binding to the active site of a catalyst, normally, but not always, leading to cleavage of that bond, whereas “functionalisation” occurs when a hydrogen is replaced with a non-hydrogen atom or group of atoms, commonly oxygen in paraffin oxidation.[9] Oxidation of paraffins is usually dominated by radical pathways in which case a hydrogen atom is removed,[8] thus forming a radical which is functionalised to give rise to the product. The efficiency of these radical reactions is generally associated with the strength of the C–H bond, therefore since the terminal position of the alkane is regarded as the least reactive (because of it containing the strongest bond in the alkane), terminal products are least likely to form.[8] This is one of the downfalls of most radically initiated paraffin oxidation processes, due to the fact that terminal products are greater in demand.

There are two types of catalysts that can be utilised for the activation of paraffins. The first is a heterogeneous system where the catalyst is in a different phase from the substrate and products, most commonly the catalyst is a solid and the substrate and products are in liquid or gas phase. The second is a homogeneous system in which the catalyst, substrate and products are all in the same phase, usually a solution phase. For the purpose of this discussion, only the latter will be emphasised. The most ideal catalyst would be one that is able to selectively insert a single oxygen atom to an activated paraffin with little to no side reactions or side products, however available data to date have shown that attaining such a catalyst is no easy task.

1.3 Transition metal complexes as catalysts for paraffin activation

Much research has been carried out regarding the use of transition metal complexes for the activation of paraffins where the active site is a vacant coordination site at the metal centre. The development of metal complexes as catalysts for paraffin activation dates back to the mid 1960’s.[10] Since then, a variety of metal complexes, some of which are highlighted in subsequent sections of this dissertation have been developed that exhibit activity in paraffin or C–H activation.

The C−H bond on a saturated hydrocarbon needs to be broken or cleaved in order for the paraffin to be activated. There are three possible mechanisms of C−H bond cleavage by metal complexes described by Shilov and Shul'pin.[11] The first mechanism involves the formation of a metal−carbon bond and cleavage of the C−H bond occurs via oxidative addition (eq 1.1), in the second mechanism cleavage of the C−H bond occurs but there is no metal−carbon bond formation and the final mechanism involves the metal complex activating a particular reagent which then in turn attacks the hydrocarbon.[11] To determine the mechanism followed will depend on the type of metal complex involved.

$$L_nM + R{-}H \longrightarrow L_nM(H{-}R) \longrightarrow L_nM(R)(H) \qquad \textbf{1.1}$$

One of the first metal complexes reported with evidence of C−H bond activation was in 1965 by Chatt.[10b] This reaction involved a Ru(0)(dmpe)$_2$ complex (Scheme 1.2) which activated C−H bonds on naphthalene (a) or directly on a phosphinomethyl group (b), as examples of oxidative addition described in eq 1.1.[10a] However, one of the earliest examples of paraffin activation (based on eq 1.1) was discovered by Crabtree in 1979 via an iridium based complex which involved the dehydrogenation of the alkane to form an alkene.[12]

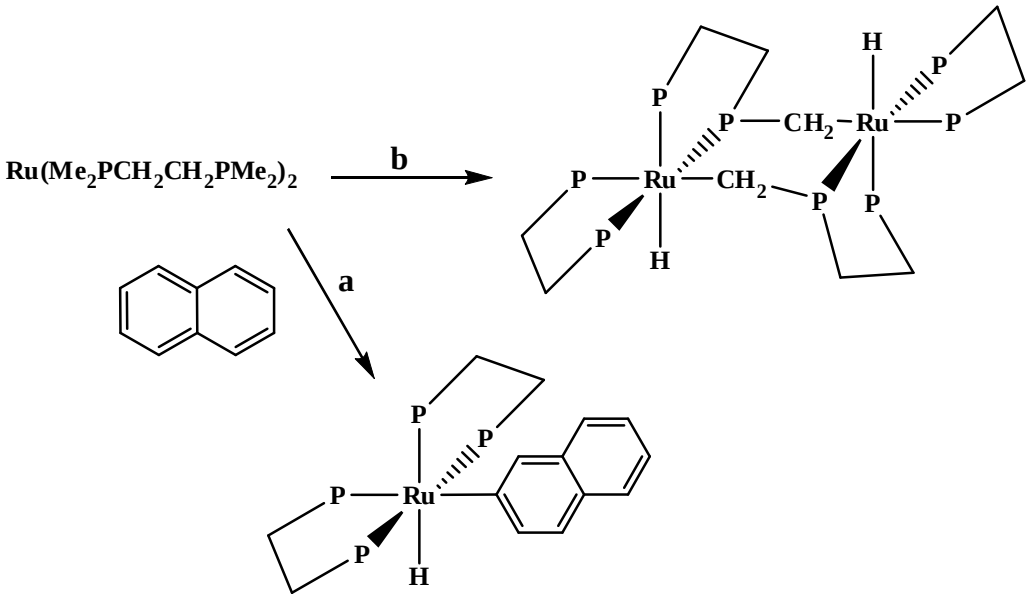

Scheme 1.2: The activation of C−H bonds by Ru(0)(dmpe)$_2$ with (a) showing the activation if naphthalene and (b) showing the activation of a phosphinomethyl group.[10a]

In paraffin oxidation, the activation step is followed by the insertion of a single oxygen atom from an appropriate donor to the activated paraffin to give rise to the functionalised product. The most common oxygen donors, also known as oxidants, are hydrogen peroxide, *tert*-butyl hydroperoxide or molecular O_2. There are cases, mostly involving metal oxo species, in which oxygen ligands on the metal directly serve as the oxidant. As shown in eq 1.2 the first step involves hydrogen abstraction from the hydrocarbon, thus forming a radical which then in turn reacts with the hydroxyl group on the metal forming the product alcohol.[11] This is an example of mechanism two discussed previously, where a definite metal−carbon bond is not actually formed.

$$RH + O{=}M^{n+} \longrightarrow R^{\bullet} + HO{-}M^{(n-1)+} \longrightarrow ROH + M^{(n-2)+} \qquad \textbf{1.2}$$

One of the earliest discoveries of paraffin oxidation was made by Shilov and co-workers in 1972, as cited numerously in the literature,[10a,11,13] who found that platinum(II) salts were able to homogeneously catalyse the activation of hydrocarbons in solution. These Pt(II) complexes converted methane to methanol under mild conditions and a proposed mechanism by Goldman and Goldberg is found in Scheme 1.3.

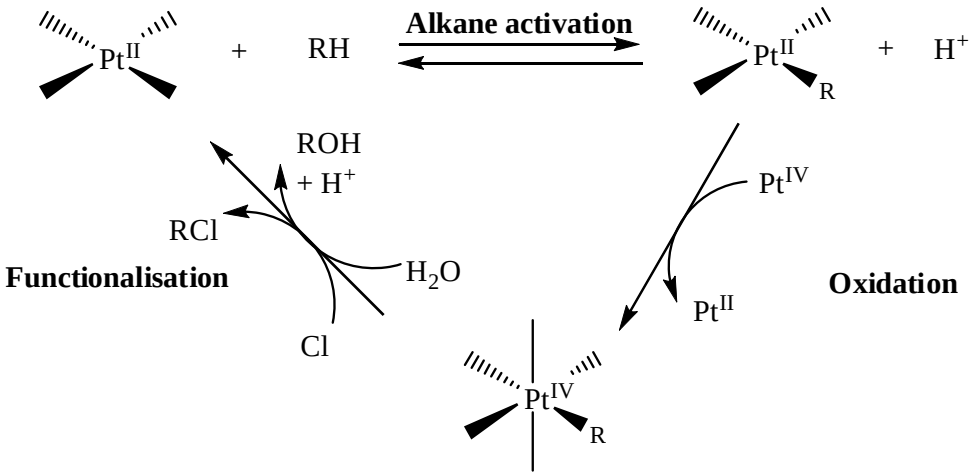

Scheme 1.3: The proposed general mechanism for the oxidation of alkanes by Shilov's platinum salts adapted from Goldman and Goldberg.[10a]

The first step involves the formation of the methylplatinum(II) intermediate upon reaction with the alkane (RH), after which there is an oxidation step leading to the oxidised methylplatinum(IV) species. In the third step, one of two possible scenarios were suggested: either there occurs a reductive elimination involving the methylplatinum(IV) species and coordinated H_2O/Cl^-; or an external nucleophile (H_2O or Cl^-) attacks the carbon, to produce the functionalised product and regenerate the platinum(II) species.[10a]

1.3.1 The use of pincer complexes for catalytic C–H activation

In addition to the aforementioned complexes, another popular choice for catalytic C–H activation is the application of complexes containing chelating multi atom pincer type ligands. The most applied pincer ligands in this category are generally terdentate ligands that coordinate to a metal centre via three atoms. If the donor atoms on the ligand are carbon atoms then a metal–carbon σ bond is usually formed.[14] This metal−carbon σ bond prevents the dissociation of the ligand from the metal, even at high temperatures, which in turn causes the complex to be thermally robust, thus leading to high turnover numbers.[15]

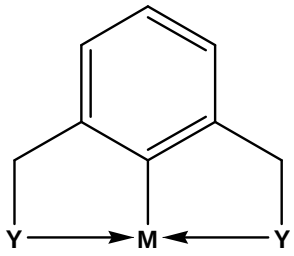

Figure 1.2: General structure of a common terdentate pincer ligand.

The most common type of pincer ligand contains an aromatic ring that forms one σ bond with the metal and the groups that are *ortho* to this bond coordinate to the metal via hetero atoms such as O, N, S or P (Fig. 1.2).[14] In general cases, the hetero atoms *ortho* to the σ bond are identical i.e. in a YCY pincer ligand system the possibilities may be:

- NCN
- PCP
- SCS

However, asymmetry may be introduced by synthesising pincer ligands that have two different hetero atoms at the *ortho* position, for example PCO and PCN.[16] There are also pincer skeletons containing CNC, in which case there are two metal–carbon σ bonds.[14] Finally, there may be instances where all the substituents are hetero atoms, in which case there are no metal–carbon σ bonds at all, e.g. a PNP ligand (Fig. 1.3).

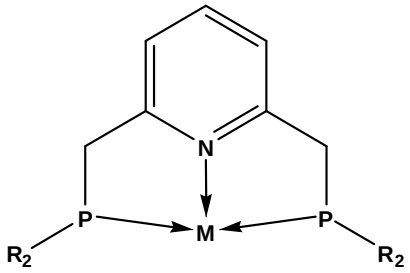

Figure 1.3: General representation of a PNP pincer ligand

The nature of the interaction between the donor atoms and the metal is very important as it determines the type of metal−ligand (M−L) coordination that results. The M−L combination also determines if a coordination compound will form, for instance, the interaction between hard metals and soft donors is unlikely to occur. This is typical with early transition metals and soft donors like sulfur, in which case any M−L coordination bond is relatively weak or labile and ligand dissociation is most likely to take place. Late transition metals are known to be soft metals and therefore would interact strongly with soft donors like sulfur.

A labile ligand is one that forms weak coordinative bonds with the metal and can easily be detached during a reaction thus rendering the catalyst unstable. On the contrary, if the ligand is bound too strongly to the metal, it may not be flexible enough and this can hinder the activity of the catalyst, which is also an undesirable property. A good ligand is one that is hemilabile so as to create coordination sites for substrates and also stabilise the catalyst and reaction intermediates in a catalytic cycle.[17]

The chelating effect of pincer ligands towards achieving hemilability, is a critical key feature to be considered in their design. Having a terdendate binding mode, these ligands are able to stabilise the metal complex more effectively when compared to mono and bidentate ligands. The occupation of three metal coordination sites by the ligand also offers greater control in terms of accessibility to the metal centre, which in turn affects binding of substrates to the metal, thus providing an advantage in catalysis.

A few examples of pincer complexes that are known for catalytic C−H activation are complexes of Ir, Ru, and Pd containing a PCP ligand,[16] as well as Ir PNP[18] complexes. In this instance C−H activation does not necessarily mean paraffin activation, therefore all the fore mentioned complexes are not particularly involved in the activation of alkanes, but rather C−H bonds of aryls, alkenes or cycloalkanes. Another example is the C−H activation of benzene, illustrated by Harkins and Peters, with an NNN pincer complex of platinum shown in Scheme 1.4.[19]

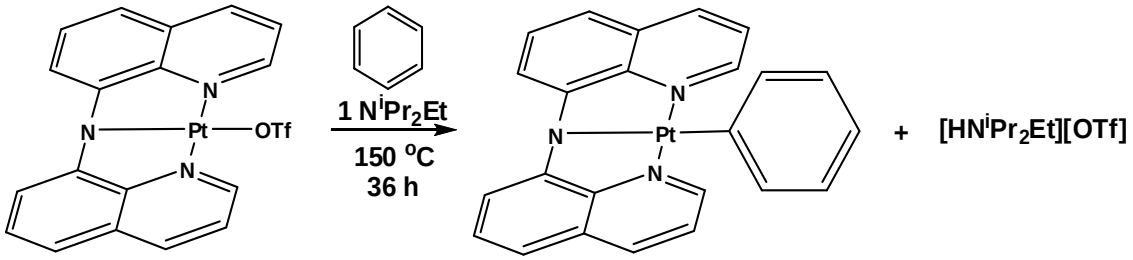

Scheme 1.4: The C−H activation of benzene by a Pt(NNN) complex.[19]

1.3.2 Catalyst design for paraffin activation

Pincer complexes are designed bearing in mind that in order to serve as a potentially good catalyst for paraffin oxidation, at some stage during the catalytic cycle of catalysis, the complex needs to be coordinatively unsaturated i.e. there must be a vacant coordination site (VCS) at the metal centre for the substrate to bind. For a coordinatively saturated complex, at least one of the bound ligands should be labile to create a VCS during the catalytic cycle.

Furthermore, ligands are selected to help regulate the activity of the metal centre. Some ligands affect the electronic properties of the metal centre, while others are used primarily for their steric bulk. When the catalytic steps involve oxidative addition, then coordinative unsaturation becomes important. Also, if there are electron rich donor atoms coordinated to the metal, then this increases the electron density at the metal centre causing increased back donation to the other ligands and strengthening the bonds between the metal and these ligands.

The steric nature of the ligands will determine how the substrate approaches the VCS, for example, sterically bulky ligands, to a certain extent, restrict access to the VCS which

dictates the direction and selectivity of the reaction towards the less hindered product. Ligands that are less bulky have reduced ability to control accessibility to the metal centre which leads to a higher conversion but loss in selectivity. The most ideal ligand offers sufficient, but controlled, access to the metal centre such that a higher conversion and selectivity of the catalyst is achieved.

1.4 SNS pincer complexes

SNS pincer complexes have received relatively less attention when compared to other pincer type complexes. However, since the discovery of SNS complexes of Mo[20] and Cr[21] as excellent ethylene trimerisation catalysts, interest in SNS ligands has increased amongst researchers with interest in pincer type ligands and complexes. To date SNS pincer complexes of Pt,[22] Pd,[23] Cr,[21] Mo,[20] Ru,[24] Cu,[25] Ni,[26] and Zn[27] have been successfully synthesised and characterised.

SNS ligands, to a certain extent, are biomimetic due to the fact that both sulfur and nitrogen are found in many biological components. The amino acids cysteine, cystine, and methionine, as well as vitamins like thiamine and biotin, are just a few examples that contain sulfur, while nitrogen is found in all amino acids and nucleic acids (RNA and DNA). With inspiration from enzymes like vitamin B_{12} (Fig. 1.4)[28] and monoxygenases[7] this research will attempt to combine SNS ligands with common metals found in biological systems, namely Fe and Co, to synthesise potential catalysts for paraffin activation and functionalisation.

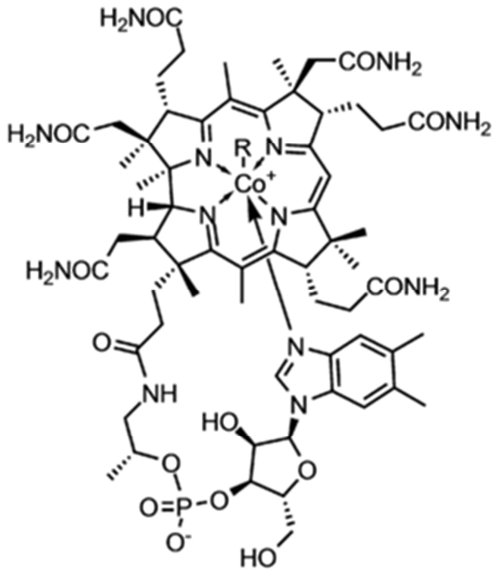

Figure 1.4: The structure of vitamin B_{12} showing the Co metal centre coordinated to nitrogen groups.[28]

A variety of advantages arise from coupling metals like Fe and Co with SNS ligands. Firstly, Fe and Co are relatively economical and low in toxicity compared to heavier transition metals like Ir, Ru and Rh, and as noted before these metals, as well as sulfur and nitrogen, are already abundant in nature and play vital roles in biological processes. Thus, this research will open up new opportunities for creating catalysts that are eco-friendly and catalytically active for paraffin oxidation. Although pincer complexes of Fe and Co are known, to the best of our knowledge there are no reported SNS pincer complexes of these metals. Reported applications of SNS ligands, including structural elucidations, are further elaborated below.

1.4.1 Selected applications of SNS pincer complexes

SNS complexes of Cu have been found useful in the Cu(I)-catalysed azide−alkyne cycloaddition (CuAAA) click reaction.[25] Bai and co-workers incorporated bis(2-(benzylthio)ethyl)amine and Cu, together with varying other ligands, and found that these complexes were catalytically active in a CuAAA three-component click reaction of benzyl chloride, sodium azide and phenylacetylene.[25] The product, 1-benzyl-4-phenyl-1*H*-1,2,3-triazole was formed in good isolated yields and the reaction proceeded without the use of a reducing agent or a base.[25]

As previously mentioned, SNS complexes of Mo[20] and Cr[21] have been highly effective as catalysts for the trimerisation of ethylene to 1-hexene. Although PNP complexes of Cr(III) have been reported as efficient catalysts for this transformation, the high costs involved in the preparation of these ligands proved to be a concern and thus McGuinness and co-workers opted for the more economically efficient SNS ligands which were found to exhibit satisfactory catalytic activity and selectivity.[21]

Brain imaging is yet another interesting application of SNS ligands which is becoming increasingly popular in the literature.[29] One of the components of a brain imaging agent is a chelating unit to which the radioactive metal centre or radionuclide is bound,[30] hence the terdentate SNS ligand serves as an ideal chelating unit. Both rhenium ($^{186/188}$Re) and technetium (^{99m}Tc) have been employed as the radionuclide and successful complexations of the SNS ligand to these metal centres have been achieved.[29] Complexes of ^{99m}Tc and a tertiary aminodithiol ligand containing the SNS donor set demonstrated high initial brain uptake in mice.[29a]

Recently, Bai and Hor discovered that Pd complexes containing the SNS donor set are useful as catalysts for Suzuki coupling.[31] They investigated two amine-based SNS ligands: bis-(2-(*i*-butylsulfanyl)ethyl)amine and bis-(2-(benzylsulfanyl)ethyl)amine, both of which were complexed to Pd(II) and found to display an unusual "ladder-like" polymeric arrangement in the hydrated form. These complexes were able to promote Suzuki-Miyaura coupling reactions of phenylboronic acid and selected heterocyclic bromides in water at 75 °C. Bai and Hor suggested that organic-based pincer type ligands like SNS have great potential in the field of water-based catalysis.[31]

1.4.2 Crystal structures of some SNS complexes

There are many reported structures of SNS ligand containing complexes in the literature. The very first terdentate SNS complex was reported in 1986 by Teixidor *et al.* where a pyridine based, thioether SNS donor set was incorporated with Zn as the metal.[27] Zn is a late transition metal and therefore can be regarded as fairly soft in nature, hence able to interact with the soft S-donor atoms. The 5-coordinate complex exhibited a trigonal bipyramidal geometry around the metal centre (Fig. 1.5). The bromide ligands were *cis* and occupied two equatorial positions, while the terdentate ligand occupied the remaining three sites via the nitrogen and two sulfur donor atoms. It was found that the N–Zn and average S–Zn bond

lengths were 2.1 and 2.7 Å respectively.[27] The S−Zn bond length was somewhat long and this was an indication of a relatively weak bond.

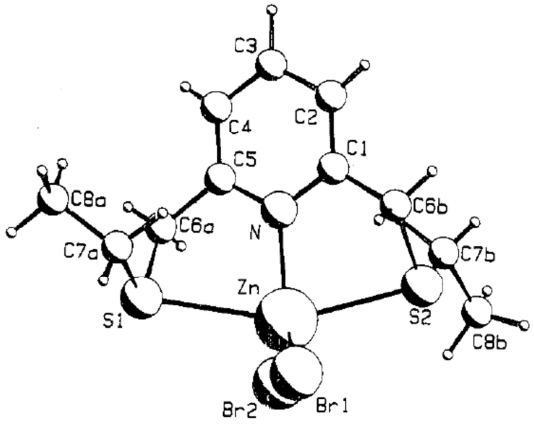

Figure 1.5: PLUTO diagram of Zn(2,6-bis((ethylthio)methyl) pyridine)Br_2.[27]

In contrast to the Zn(SNS) complex, Downing and co-workings[20] reported an octahedral Mo(III) complex containing an amine-based SNS ligand, namely bis(2-ethylthioethyl)amine represented in Fig. 1.6.

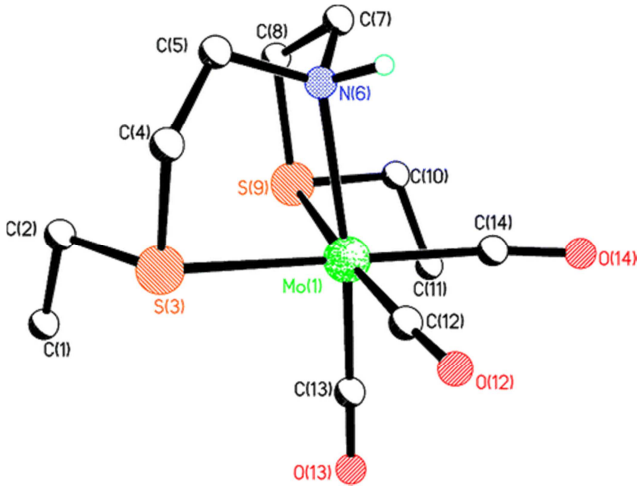

Figure 1.6 :ORTEP diagram of Mo(bis(2-(ethylthioethyl)amine)Cl_3.[20]

The crystal structure for this complex displayed meridional coordination of the SNS ligand with syn-geometry and an average S–Mo bond length of 2.5 Å,[20] which was slightly shorter than the aforementioned S–Zn bond length. The N–Mo and N–Zn bond lengths are quite

similar at 2.2 and 2.1 Å respectively, despite the fact that the nitrogen source is completely different i.e. an amine and a pyridine respectively.

Temple *et al.* also reported crystal structures of the popular Cr(SNS) trimerisation catalysts (Fig. 1.7) which shows that the complex also exists as a six coordinate octahedron.[32] The bond length found for Cr−N was 2.1 Å which is again quite similar to that of the complexes discussed above, while the average Cr−S bond length was 2.4 Å.

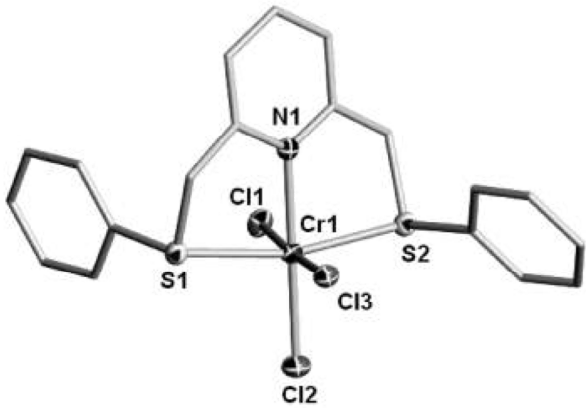

Figure 1.7: X-ray crystal structure of Cr(2,6-bis(phenylthioethyl)pyridine)Cl_3.[32]

A very interesting Ir(SNS) crystal structure was reported by Klerman *et al.* (Fig. 1.8) which displayed a distorted square planar geometry around Ir(I).[33] The substituents on the S-donor atoms were *t*-butyl groups which were positioned at different sides of the SNS plane while the cyclooctene (COE) substituent was found to be almost perpendicular to the SNS plane. The Ir−N and average Ir−S bond lengths were 2.0 Å and 2.3 Å respectively and when these values are compared to those of Zn, Mo and Cr, it can be said that the Ir−N and Ir−S bonds are much stronger, since the bond lengths are relatively shorter. Given the fact that Ir is a late transition metal and thus is a softer metal, the SNS ligand interacts strongly in a soft-soft combination, because of the softer nature of the donor atoms.

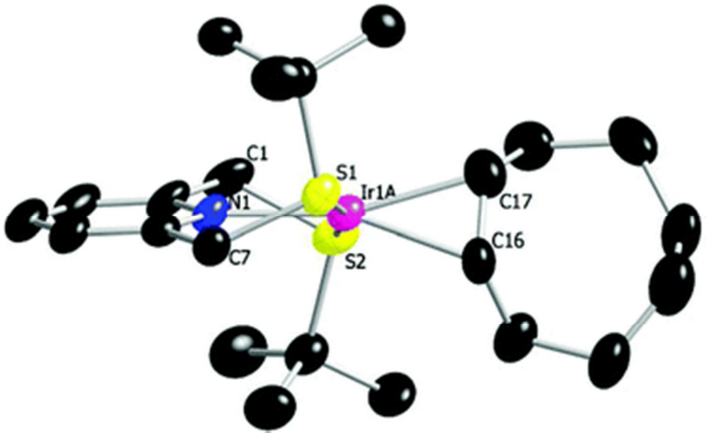

Figure 1.8: ORTEP diagram of Ir(2,6-bis(phenylthioethyl)pyridine)(COE)(BF_4).[33]

From these it can be concluded that the bond between the metal and N does not differ by much with respect to the type of metal or source of N, however the substituents on the S-donor atoms have an effect on the metal−S bond and hence the strength of the bond as illustrated by the varying bond lengths displayed by the crystal structures of the compounds discussed.

1.5 Project aims and goals

The main aims of this project are to firstly synthesise and characterise a range of SNS ligands, complex these ligands to iron and cobalt and finally test the catalytic activity of these pincer complexes as potential paraffin oxidation catalysts. In order to determine the choice of the catalyst, the choice of SNS ligand had to be given some thought. Two different sources of nitrogen were chosen for investigation to determine how this would potentially affect the activity of the catalyst: a constrained six membered pyridine ring and a linear straight chained amine.

The preferred choice is to have an unsaturated complex as shown in Fig. 1.9 where the geometry around the metal centre is trigonal bypyrimidal, therefore during the catalytic cycle the complex can transform into an octahedral geometry when the substrate binds. The R groups on the sulfur atoms can also be varied to investigate the electronic and steric effects of the catalyst.

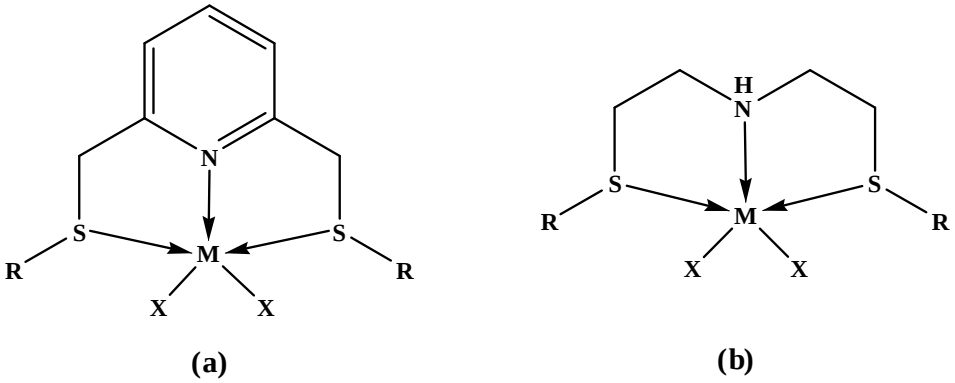

Figure 1.9: Structures of the SNS pincer complexes with the nitrogen source as a pyridine (a) or an amine (b).

The ultimate goal of this project was to create a catalyst that is biomimetic, eco-friendly, as well as economical. Being biomimetic, the catalysts will be able to function at relatively milder conditions when compared to other catalytic systems that require high temperatures and pressures in order to produce satisfactory results. The choice of metal was very important and therefore with much consideration iron and cobalt were chosen, since both of these metals fit the required criteria.

1.5.1 Thesis scope and contents

This thesis outlines and explains in detail the preparation of SNS ligands and subsequent complexes, as well as their application in paraffin oxidation. Chapter 2 is dedicated to the synthesis and characterisation of the ligands and respective complexes, describing in detail the synthetic protocols followed and the results obtained for each characterisation technique to ensure successful synthesis of the target compound. The structural aspects of selected complexes are then described in Chapter 3, where crystal structures are presented and discussed with emphasis placed on bond lengths, bond angles and the geometry displayed by the complexes. Chapter 4 details the catalytic results obtained for the various catalysts prepared, in the oxidation of *n*-octane to oxygenated products such as octanone, octanol, octanal and octanoic acid. In this chapter, the conversion and selectivity of each catalyst is calculated and discussed and the most efficient catalytic system is determined from the results. The thesis culminates with a summary and the conclusions drawn from the all results obtained, in Chapter 5.

References

(1) Breslow, R. *Accounts of Chemical Research* **1995**, *28*, 146.

(2) Burrington, J. D. In *Biocatalysis and Biomimetics*; American Chemical Society, 1989; Vol. 392.

(3) Torres Pazmino, D. E.; Winkler, M.; Glieder, A.; Fraaije, M. W. *Journal of Biotechnology* **2010**, *146*, 9.

(4) Guengerich, F. P. *Chemical Research in Toxicology* **2001**, *14*, 611.

(5) Costas, M.; Chen, K.; Que Jr., L. *Coordination Chemistry Reviews* **2000**, *200-202*, 517.

(6) Fish, R. H.; Oberhausen, K. J.; Chen, S.; Richardson, J. F.; Pierce, W.; Buchanan, R. M. *Catalysis Letters* **1993**, *18*, 357.

(7) Westerheide, L.; Pascaly, M.; Krebs, B. *Current Opinion in Chemical Biology* **2000**, *4*, 235.

(8) Labinger, J. A.; Bercaw, J. E. *Nature* **2002**, *417*, 507.

(9) Crabtree, R. H. *Journal of the Chemical Society, Dalton Transactions* **2001**, 2437.

(10) (a) Goldman, A. S.; Goldberg, K. I. In *Activation and Functionalization of C- H Bonds*; American Chemical Society, 2004; Vol. 885. (b) Chatt, J.; Davidson, J. M. *Journal of the Chemical Society (Resumed)* **1965**, 843.

(11) Shilov, A. E.; Shul'pin, G. B. *Chemical Reviews* **1997**, *97*, 2879.

(12) (a) Crabtree, R. H.; Mihelcic, J. M.; Quirk, J. M. *Journal of the American Chemical Society* **1979**, *101*, 7738. (b) Crabtree, R. H.; Mellea, M. F.; Mihelcic, J. M.; Quirk, J. M. *Journal of the American Chemical Society* **1982**, *104*, 107.

(13) Crabtree, R. H. *Journal of Organometallic Chemistry* **2004**, *689*, 4083.

(14) Singleton, J. T. *Tetrahedron* **2003**, *59*, 1837.

(15) Carlson, A. R., Master of Science thesis, University of Florida, 2007.

(16) van der Boom, M. E.; Milstein, D. *Chemical Reviews* **2003**, *103*, 1759.

(17) Braunstein, P.; Naud, F. *Angewandte Chemie International Edition* **2001**, *40*, 680.

(18) Meiners, J.; Friedrich, A.; Herdtweck, E.; Schneider, S. *Organometallics* **2009**, *28*, 6331.

(19) Harkins, S. B.; Peters, J. C. *Organometallics* **2002**, *21*, 1753.

(20) Downing, S. P.; Hanton, M. J.; Slawin, A. M. Z.; Tooze, R. P. *Organometallics* **2009**, *28*, 2417.

(21) McGuinness, D. S.; Wasserscheid, P.; Keim, W.; Morgan, D.; Dixon, J. T.; Bollmann, A.; Maumela, H.; Hess, F.; Englert, U. *Journal of the American Chemical Society* **2003**, *125*, 5272.

(22) Pitteri, B.; Bortoluzzi, M. *Polyhedron* **2008**, *27*, 2259.

(23) Canovese, L.; Chessa, G.; Marangoni, G.; Pitteri, B.; Uguagliati, P.; Visentin, F. *Inorganica Chimica Acta* **1991**, *186*, 79.

(24) Viñas, C.; Anglès, P.; Sánchez, G.; Lucena, N.; Teixidor, F.; Escriche, L.; Casabó, J.; Piniella, J. F.; Alvarez-Larena, A.; Kivekäs, R.; Sillanpää, R. *Inorganic Chemistry* **1998**, *37*, 701.

(25) Bai, S.-Q.; Koh, L. L.; Hor, T. S. A. *Inorganic Chemistry* **2009**, *48*, 1207.

(26) Konrad, M.; Meyer, F.; Heinze, K.; Zsolnai, L. *Journal of the Chemical Society, Dalton Transactions* **1998**, 199.

(27) Teixidor, F.; Escriche, L.; Casabo, J.; Molins, E.; Miravitlles, C. *Inorganic Chemistry* **1986**, *25*, 4060.

(28) http://upload.wikimedia.org/wikipedia/commons/thumb/e/ec/Cobalamin.png/280px-Cobalamin.png., date accessed: 01/11/2011.

(29) (a) Mastrostamatis, S. G.; Papadopoulos, M. S.; Pirmettis, I. C.; Paschali, E.; Varvarigou, A. D.; Stassinopoulou, C. I.; Raptopoulou, C. P.; Terzis, A.; Chiotellis, E. *Journal of Medicinal Chemistry* **1994**, *37*, 3212. (b) Papadopoulos, M. S.; Pirmettis, I. C.; Pelecanou, M.; Raptopoulou, C. P.; Terzis, A.; Stassinopoulou, C. I.; E., C.

Inorganic Chemistry **1996**, *35*, 7377. (c) Chen, X.; Femia, F. J.; Babich, J. W.; Zubieta, J. *Inorganica Chimica Acta* **2000**, *307*, 88. (d) Nock, B. A.; Maina, T.; Yannoukakos, D.; Pirmettis, I. C.; Papadopoulos, M. S.; Chiotellis, E. *Journal of Medicinal Chemistry* **1999**, *42*, 1066.

(30) Meltzer, P. C.; Blundell, P.; Jones, A. G.; Mahmood, A.; Garada, B.; Zimmerman, R. E.; Davison, A.; Holman, B. L.; Madras, B. K. *Journal of Medicinal Chemistry* **1997**, *40*, 1835.

(31) Bai, S.-Q.; Hor, T. S. A. *Chemical Communications* **2008**, 3172.

(32) Temple, C. N.; Gambarotta, S.; Korobkov, I.; Duchateau, R. *Organometallics* **2007**, *26*, 4598.

(33) Klerman, Y.; Ben-Ari, E.; Diskin-Posner, Y.; Leitus, G.; Shimon, L. J. W.; Ben-David, Y.; Milstein, D. *Dalton Transactions* **2008**, 3226.

CHAPTER TWO

The preparation of SNS ligands and complexes

2.1 Introduction

This chapter describes the synthetic routes followed for the preparation of the SNS ligands and corresponding metal complexes. It also details the characterisation techniques employed for the analyses and discusses the results obtained.

SNS ligands, sometimes referred to as hybrid ligands,[1] are so named because they are composed of two sulfur and one nitrogen donor atoms. Generally, these pincer ligands are terdentate which means that three coordinative bonds are formed between the metal and donor atoms. However, complexes bearing bidentate SNS ligands have been reported in the literature.[2] In these ligands, the nitrogen atom is usually hard while the sulfur atoms are soft donors[3] thus making it difficult for the sulfur component of the SNS ligand to coordinate to early transition metals which are considered as hard metal centres.

One of the key features of the SNS pincer ligand relevant to its application in catalysis, is that it may be designed to adopt a hemilabile nature.[4] Being hemilabile also affords a balance between stability and reactivity of the metal complex.[4] The concept of hemilability can be described as a polydentate ligand system equilibrating between two different modes: coordination (closed) or dissociation (open), dependent on the donor strengths of the atoms in the polydentate system.[5] Therefore, the S-donor atoms are the hemilabile components of an SNS ligand as a result of their possession of soft and relatively weak donor qualities.

In the design of an SNS ligand system, the important components to be considered are the sources of the N-donor atom and the substituents on the S-donor atoms. The fact that the SNS moiety is easily modified offers a tremendous advantage in catalysis, since the ligand may be tuned to suit the desirable properties of the complex and the reactivity and stability of the final catalyst may be adjusted. SNS ligand tuning may be achieved by variations of the nitrogen source, substituents bonded to the S-donor atoms, as well as adjustments to the nature and type of the linker that bonds the N and S atoms.

A variety of nitrogen donors have already been investigated for the synthesis of SNS ligands, including heterocycles like pyrroles,[6] pyridines,[7] imidazoles,[8] as well as non-heterocyclic donors like amines[1,9] and imines[10]. The most common of these nitrogen sources are the pyridines and amines, from which a range of complexes have been reported. This project will study two types of SNS ligands, one with a pyridine backbone and the other with an amine backbone, to investigate the effect that the backbone has on the activity of the catalyst.

2.1.1 Pyridine-based SNS ligands

The pyridine-based ligands have a constrained, six-membered pyridine ring as the backbone of the ligand with the sulfur donor atoms bonded at the 2- and 6- positions on the ring usually via a methyl linker (Fig. 2.1). In this project, five different pyridine-based SNS ligands have been prepared by varying the substituents attached to the S-donor atoms i.e. methyl (me), ethyl (et), butyl (but), cyclohexyl (cy) and phenyl (ph) groups. Henceforth, for ease of referencing, the abbreviations given to these ligands will be SNS-Rpy, with R referring to the substituent on the S-donor atoms.

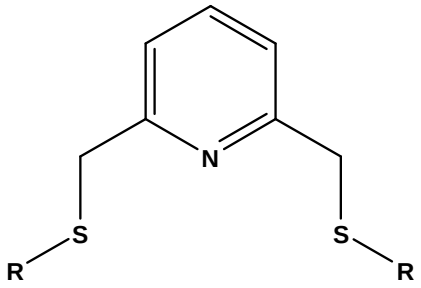

Figure 2.1: The general structure of the pyridine-based SNS ligands (SNS-Rpy).

2.1.2 Amine-based SNS ligands

The amine-based ligands have a linear, straight chained amine backbone with an ethylene linker between the N- and S-donor atoms (Fig. 2.2). A total of three amine-based ligands have been prepared with the substituents on the S-donor atoms being et, but and decyl (dec). Henceforth, the abbreviations given to these ligands will be SNS-Ramine with R referring to the corresponding S-donor substituent.

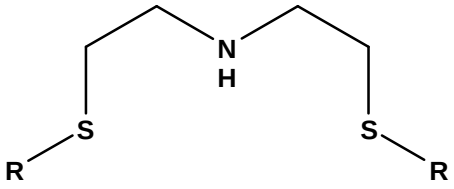

Figure 2.2: The general structure of the amine-based SNS ligands (SNS-Ramine).

2.2 Experimental

2.2.1 Materials

The synthesis of all ligands and complexes were performed under inert nitrogen atmosphere using standard Schlenk techniques and unless otherwise stated, solvents were dried according to established methods. Diethyl ether (Et_2O) and tetrahydrofuran (THF) were dried over sodium wire and benzophenone, absolute ethanol (EtOH) was dried over magnesium turnings/iodine, and dichloromethane (DCM) was dried over phosphorous pentoxide. All solvents were freshly distilled prior to use. High purity nitrogen gas was purchased from Afrox. Sodium methanethiolate (90%), ethanethiol (97%), cyclohexyl mercaptan (97%), bis-2(chloroethyl)amine hydrochloride (98%), and 2,6-pyridinedimethanol (98%) were purchased from Sigma-Aldrich. Butanethiol (97%) and decanethiol (95%) were purchased from Fluka. Thiophenol (99%), 4-toluenesulfonyl chloride (98%), and sodium hydroxide (98%) were sourced from Merck. Cobaltous chloride (99%) was obtained from Associated Chemical Enterprises. All chemicals were used as received from the various sources.

2.2.2 Instrumentation

NMR spectroscopy was employed to elucidate and confirm the structures of the ligands. All NMR spectra were recorded using a Bruker Avance III 400 MHz spectrometer at ambient temperature. The ^{1}H NMR data are reported as: chemical shift (δ, ppm) and referenced to the solvent peak $CDCl_3$ (7.26 ppm); multiplicity and number of protons are presented in parentheses. The proton decoupled ^{13}C NMR data are presented as: chemical shift (δ, ppm) and referenced to the solvent peak $CDCl_3$ (77.16) with the specific carbon indicated in parentheses. The ^{13}C DEPT 135 NMR data, which distinguishes between CH, CH_2 and CH_3,

are listed as: chemical shift (δ, ppm) and positive (pos) or negative (neg) with the corresponding carbons in parentheses.

Infrared (IR) spectroscopy was carried out to investigate the vibrational modes of the functional groups of the ligands and complexes which in turn gave information about the structure of the compound. The IR spectra were recorded on a Perkin Elmer Attenuated Total Reflectance (ATR) spectrophotometer with only the significant bands reported in cm^{-1}. Elemental analysis was employed to determine the elemental composition as well as the purity of the complexes, and this was performed on a LECO CHNS elemental analyser. Another technique to determine the purity of the complexes is to obtain the melting point and this was performed using a Stuart Scientific melting point apparatus. High resolution mass spectrometry was utilised to determine the mass-to-charge ratio (m/z) of the compounds, thus in turn obtaining the total mass of the compound for the confirmation of the structure. The high resolution mass spectrometric data were collected using a Bruker Micro TOF-Q11 (where TOF is Time of Flight) with electron spray ionisation (ESI) and a sample concentration of approximately 1 ppm.

2.2.3 Experimental protocols

2.2.3.1 Preparation of pyridine-based ligands

Precursor 2,6-pyridine-dimethylene-ditosylate

Reported protocols for the preparation of the pyridine-based ligands involve expensive starting materials like 2,6-bis(chloromethyl)pyridine, therefore an alternate synthetic route was followed to reduce the costs. A more suitable starting material, 2,6-pyridine-dimethylene-ditosylate (PMT), was employed which involves the use of cheaper reagents to prepare, and the method followed was adapted from Reger *et al.*[11] To a 500 ml round bottom flask (RBF), a solution containing 8.0 g (0.20 mol) of NaOH and 2.78 g (0.020 mol) of 2,6-pyridinedimethanol was prepared in 150 ml THF/water (1:1). The solution was then cooled to 0 °C to which a mixture of *p*-toluenesulfonyl chloride in 75 ml of THF was added. After stirring at room temperature for four hours, the mixture was poured into 200 ml of water and extracted with 75 ml of dichloromethane (DCM) and this was repeated three times. The organic phase was washed with a saturated NaCl solution and distilled water, and dried with

Na_2SO_4. The solvent was removed under vacuum yielding a crystalline white product (6.57 g, 73%). ^{1}H NMR (400 MHz, $CDCl_3$): δ 2.4 (s, 6H), 5.1 (s, 4H), 7.3 (d, 6H), 7.7 (t, 1H), 7.8 (d, 4H).

2,6-Bis(methylthiomethyl)pyridine (SNS-mepy)

To prepare this ligand a modified protocol adapted from Canovese *et al.* was followed.[7a] To a 50 ml two neck RBF fitted with a nitrogen tap, a mass of 1.79 g of PMT was dissolved in ~40 ml of THF and this solution was cooled in an ice bath. A mass of 0.62 g of sodium methanethiolate was added to the ice cooled solution after which the mixture was stirred for 2 hours at room temperature. At the end of the reaction the solvent was evacuated under reduced pressure and the resulting cream residue was partitioned between DCM (200 ml) and water (100 ml). After washing several times with water, the organic phase was dried with $MgSO_4$ and the solvent removed to yield the product as an impure pale yellow oil. The product was purified by elution with DCM through a silica packed column (0.53 g, 66%). ^{1}H NMR (400 MHz, $CDCl_3$): δ 2.0 (s, 6H), 3.8 (s, 4H), 7.2 (d, 2H), 7.6 (t, 1H). ^{13}C NMR (400 MHz, $CDCl_3$): δ 15.2 (*C*H_3-S), 40.0 (py-*C*H_2-S), 121.1 (*C*H-py), 137.3 (*C*H-py), 158.2 (*C*-py). ^{13}C DEPT 135 (400 MHz, $CDCl_3$): δ 15.2 (CH_3-S) neg, 40.0 (CH_2-S) pos, 121.1 (CH-py) neg, 137.3 (CH-py) neg. IR ν_{max} (cm^{-1}): 3058 (w), 2966 (m), 2914 (m), 2856 (m), 1589 (s), 1572 (s), 1451 (s), 747 (s), 813 (m).

2,6-Bis(ethylthiomethyl)pyridine (SNS-etpy)

The procedure followed for the synthesis of SNS-etpy was taken from Teixidor *et al.*[7c] with a few modifications. An ethanol solution (10 ml) of sodium metal (0.23 g, 10 mmol) and ethanethiol (0.5 ml, 10 mmol) was stirred together for 20 min in a 20 ml Schlenk tube. This solution was added to another ethanol solution (50 ml) of PMT (2.24 g, 5 mmol) in a 100 ml two neck RBF fitted with a nitrogen tap, and the reaction mixture was left to reflux overnight. The solvent was removed in vacuo and the residue was extracted twice with diethyl ether (150 ml), the solid residue was discarded. The extract was washed with aqueous Na_2CO_3 and twice with water (150 ml) and dried with $MgSO_4$. The solvent was removed in vacuo to yield the impure product which was purified analogously to SNS-mepy to give a pale yellow oil (0.62 g, 54%). ^{1}H NMR (400 MHz, $CDCl_3$): δ 1.2 (t ,6H), 2.5 (q,4H), 3.8 (s,4H), 7.2 (d, 2H), 7.6 (t, 1H). ^{13}C NMR (400 MHz, $CDCl_3$): δ 14.5 (*C*H_3CH_2-S), 25.6 (CH_3*C*H_2-S), 37.8 (py-

CH_2-S), 121.0 (*C*H-py), 137.2 (*C*H-py), 158.5 (*C*-py). ^{13}C DEPT 135 (400 MHz, $CDCl_3$): δ 14.5 (CH_3-S) neg, 25.6 (CH_2-S) pos, 37.8 (py-CH_2-S) pos, 121.0 (CH-py) neg, 137.2 (CH-py) neg. IR ν_{max} (cm^{-1}): 3056 (w), 2971 (m), 2926 (m), 2869 (m), 1590 (s), 1573 (s), 1451 (s), 747 (s), 788 (m).

2,6-Bis(butylthiomethyl)pyridine (SNS-butpy)

A similar procedure to that of SNS-etpy was followed for SNS-butpy with the following masses and volumes: sodium metal (0.14 g, 6.18 mmol), butanethiol (0.7 ml, 6.18 mmol), PMT (1.38 g, 3.09 mmol). No further purification was required as the TLC showed only one spot; however the oil was dried under reduced pressure for several hours to remove any present solvent, thus yielding the product as a yellow oil (0.55 g, 63%). ^{1}H NMR (400 MHz, $CDCl_3$): δ 0.9 (t, 6H), 1.4 (m, 4H), 1.6 (m, 4H), 2.5 (t, 4H), 3.8 (s, 4H), 7.3 (d, 2H), 7.6 (t, 1H). ^{13}C NMR (400 MHz, $CDCl_3$): δ 13.7 (*C*$H_3$$CH_2$$CH_2$$CH_2$-S), 22.0 ($CH_3$*C*$H_2$$CH_2$$CH_2$-S), 31.3 ($CH_3$$CH_2$*C*$H_2$$CH_2$-S), 31.4 ($CH_3$$CH_2$$CH_2$*C*$H_2$-S), 38.1 (py-*C*$H_2$-S), 121.0 (*C*H-py), 137.2 (*C*H-py), 158.5 (*C*-py). ^{13}C DEPT 135 (400 MHz. $CDCl_3$): δ 13.7 (CH_3-S) neg, 22.0 (CH_2-S) pos, 31.4 (CH_2-S) pos, 38.1 (CH_2-S) pos, 121.0 (CH-py) neg, 137.2 (CH-py) neg. IR ν_{max} (cm^{-1}): 3056 (w), 2956 (m), 2926 (m), 2871 (m), 1589 (s), 1573 (s), 1451 (s), 747 (s), 812 (m).

2,6-Bis(cyclohexylthiomethyl)pyridine (SNS-cypy)

This method was adapted from Temple *et al.*.[12] In a 20 ml Schlenk tube, NaOH (0.32 g, 8.2 mmol) and cyclohexyl mercaptan (1.0 ml, 8.2 mmol) were stirred together in ethanol (10 ml) for 30 min. This mixture was added dropwise to a THF solution (20 ml) of PMT (1.79 g, 4 mmol) in a separate 100 ml two neck RBF fitted with a nitrogen tap. After stirring at room temperature overnight, the solvent was removed in vacuo and the residue was partitioned between DCM and deionised water (50 ml each). The organic layer was collected, while the aqueous layer was washed with DCM (20 ml x 3), then the organics were combined and dried with $MgSO_4$. After the solvent was removed in vacuo the product was obtained as a yellow oil and no further purification was required (1.21 g, 91%). ^{1}H NMR (400 MHz, $CDCl_3$): δ 1.3 (m, 10H), 1.6 (m, 2H), 1.7 (m, 4H), 1.9 (m, 4H), 2.6 (m, 2H), 3.8 (s, 4H), 7.2 (d, 2H), 7.6 (t, 1H). ^{13}C NMR (400 MHz, $CDCl_3$): δ 25.9 (*C*H_2-cy), 26.1 (*C*H_2-cy), 33.5 (*C*H_2-cy), 36.6 (py-*C*H_2-S), 43.4 (*C*H-cy), 121.0 (*C*H-py), 137.3 (*C*H-py), 158.8 (*C*-py). ^{13}C DEPT 135

NMR (400 MHz. $CDCl_3$): δ 25.9 (CH_2-cy) pos, 26.1 (CH_2-cy) pos, 33.5 (CH_2-cy) pos, 36.6 (py-CH_2-S) pos, 43.4 (CH-cy) neg, 121.0 (CH-py) neg, 137.3 (CH-py) neg. IR ν_{max} (cm^{-1}): 3064 (w), 2962 (m), 2923 (m), 1590 (s), 1571 (s), 1480 (s), 1449 (s), 737 (s), 809 (m).

2,6-Bis(phenylthiomethyl)pyridine (SNS-phpy)

This method was adapted from Teixidor *et al.*.[3] Sodium metal (0.14 g, 6 mmol) was stirred with thiophenol (0.61 ml, 6 mmol) in ethanol (10 ml) in a 20 ml Schlenk tube for 10 min. The solution was then added dropwise to an ice cooled solution of PMT (1.52 g, 3 mmol) in THF (20 ml) and the resultant solution was stirred for a further three hours at 0 °C. The solvent was then removed in vacuo and the resulting residue was extracted with 70 ml diethyl ether and washed with 1 M NaOH solution (25 ml x 2) after which the organic layer was dried with $MgSO_4$. The solvent was removed in vacuo to yield the product as a pale yellow oil and no further purification was required (0.90 g, 82%). ^{1}H NMR (400 MHz, $CDCl_3$): δ 4.2 (s, 4H), 7.1 (d, 4H), 7.2 (t, 4H), 7.3 (d, 4H), 7.5 (t, 1H). ^{13}C NMR (400 MHz, $CDCl_3$): δ 40.3 (py-*C*H_2-S), 121.3 (*C*H-py), 126.2 (*C*H-ph), 128.9 (*C*H-ph), 129.6 (*C*H-ph), 135.7 (*C*-ph), 137.2 (*C*H-py), 157.3 (*C*-py). ^{13}C DEPT 135 NMR (400 MHz. $CDCl_3$): δ 40.3 (py-CH_2-S) pos, 121.3 (CH-py) neg, 126.2 (CH-ph) neg, 128.9 (CH-ph) neg, 129.6 (CH-ph) neg, 137.2 (CH-py) neg. IR ν_{max} (cm^{-1}): 3064 (w), 2962 (m), 2923 (m), 1590 (s), 1571 (s), 1450 (s), 1436 (s), 737 (s), 809 (m).

2.2.3.2 Preparation of amine-based ligands

Bis[2-(ethylthio)ethyl]amine (SNS-etamine)

The method for the preparation of SNS-etamine was adapted from Konrad *et al.*.[13] In a 250 ml Schlenk flask, a mass of 8.79 g (50 mmol) of bis(2-chloroethyl)amine hydrochloride was dissolved in 100 ml of ethanol. The solution was added to a 500 ml Schlenk flask which contained a mixture of NaOH (5.99 g, 150 mmol) and ethanethiol (11.0 ml, 150 mmol) in ethanol (150 ml) at 0 °C. The resultant mixture was stirred for two hours, filtered via canula and the filtrate was dried in vacuo. Diethyl ether was added to the residue and once again the mixture was filtered and the filtrate dried in vacuo to yield the product as a pale yellow oil (6.66g, 69%). ^{1}H NMR (400 MHz, $CDCl_3$): δ 1.3 (t, 6H), 1.8 (s, 1H, N−H), 2.6 (q, 4H), 2.7 (t, 4H), 2.8 (q, 4H). ^{13}C NMR (400 MHz, $CDCl_3$): δ 14.9 (*C*$H_3$$CH_2$-S), 25.9 ($CH_3$*C*$H_2$-S),

31.9 (*C*$H_2$$CH_2$-N), 48.3 ($CH_2$*C*$H_2$-N). ^{13}C DEPT 135 NMR (400 MHz. $CDCl_3$): δ 14.9 (CH_3-S) neg, 25.9 (CH_2-S) pos, 31.9 (CH_2-N) pos, 48.3 (CH_2-N) pos. IR ν_{max} (cm^{-1}): 3288 (w), 2962 (s), 2921 (s), 2864 (s), 2823 (s), 1451 (s), 739 (m).

Bis[2-(butylthio)ethyl]amine (SNS-butamine)

SNS-butamine was synthesised analogously to SNS-etamine with the following masses and volumes: bis(2-chloroethyl)amine hydrochloride (8.81 g, 50 mmol), NaOH (6.13 g, 150 mmol) and butanethiol (16.0 ml, 150 mmol). The product was obtained as a yellow oil (10.71 g, 86%). ^{1}H NMR (400 MHz, $CDCl_3$): δ 0.9 (t, 6H), 1.3 (m, 4H), 1.5 (m, 4H), 1.8 (s, 1H, N−H), 2.5 (t, 4H), 2.6 (t, 4H), 2.8 (t, 4H). ^{13}C NMR (400 MHz, $CDCl_3$): δ 13.7 (*C*$H_3$$CH_2$$CH_2$$CH_2$-S), 22.0 ($CH_3$*C*$H_2$$CH_2$$CH_2$-S), 31.7 ($CH_3$$CH_2$*C*$H_2$$CH_2$-S), 31.8 ($CH_3$$CH_2$$CH_2$*C*$H_2$-S), 32.4 (*C*$H_2$$CH_2$-N), 48.4 ($CH_2$*C*$H_2$-N). ^{13}C DEPT 135 NMR (400 MHz. $CDCl_3$): δ 13.7 (CH_3-S) neg, 22.0 (CH_2-S) pos, 31.7 (CH_2-S) pos, 31.8 (CH_2-S) pos, 32.4 (CH_2-N) pos, 48.4 (CH_2-N) pos. IR ν_{max} (cm^{-1}): 3294 (w), 2955 (vs), 2925 (vs), 2872 (vs), 1458 (s), 741 (m).

Bis[2-(decylthio)ethyl]amine (SNS-decamine)

SNS-decamine was synthesised analogously to SNS-etamine and SNS-butamine, however the reaction was left to stir overnight instead of two hours and the following masses and volumes were used: bis(2-chloroethyl)amine hydrochloride (8.80 g, 50 mmol), NaOH (6.01 g, 150 mmol) and decanethiol (30.9 ml, 150 mmol). The product obtained was a dark yellow to orange oil (17.69 g, 85%). ^{1}H NMR (400 MHz, $CDCl_3$): δ 0.9 (t, 6H), 1.2 (m, 28H), 1.4 (m, 4H), 1.6 (m, 4H), 1.8 (bs, 1H, N−H), 2.5 (t, 4H), 2.7 (t, 5H), 2.8 (t, 3H). ^{13}C NMR (400 MHz, $CDCl_3$): δ 14.1 (*C*H_3-dec-S), 22.7 (*C*H_2-dec-S), 28.5-32.0 (*C*H_2-dec-S), 39.2 (*C*H_2-N), 48.3 (*C*H_2-N). ^{13}C DEPT 135 NMR (400 MHz. $CDCl_3$): δ 14.1 (CH_3-dec-S) neg, 22.7 (CH_2-dec-S) pos, 28.5-32.0 (CH_2-dec-S) pos, 39.2 (CH_2-N) pos, 48.3 (CH_2-N) pos. IR ν_{max} (cm^{-1}): 2923 (vs), 2852 (vs), 1460 (s), 721 (m).

2.2.3.3 Cobalt complexes

To the best of our knowledge, there is little to no research available on cobalt-based SNS complexes, hence novel methodology was developed for the synthesis of the Co(SNS) complexes. The preparations of the complexes were based on a program of systemic trial and error and only the protocols that eventually gave the best results are reported.

(a) Pyridine-based cobalt complexes

The structures of complexes **Ia-Va** are represented in Fig. 2.3 and all relevant information for each complex can be found in Table 2.1. All complexes were prepared in a similar manner under inert atmosphere of which the general procedure is given below.

A mixture of the ligand in ethanol (5 ml) was added dropwise to a solution of $CoCl_2.6H_2O$ in ethanol (10 ml) in a 1:1 mole ratio. After an overnight reflux, the resulting indigo solution was concentrated by reducing the volume of the solvent to ~5 ml. At this point the product precipitated out, was separated via canular filtration and washed with a small amount of ethanol. Drying in vacuo for several hours afforded the product as a coloured solid.

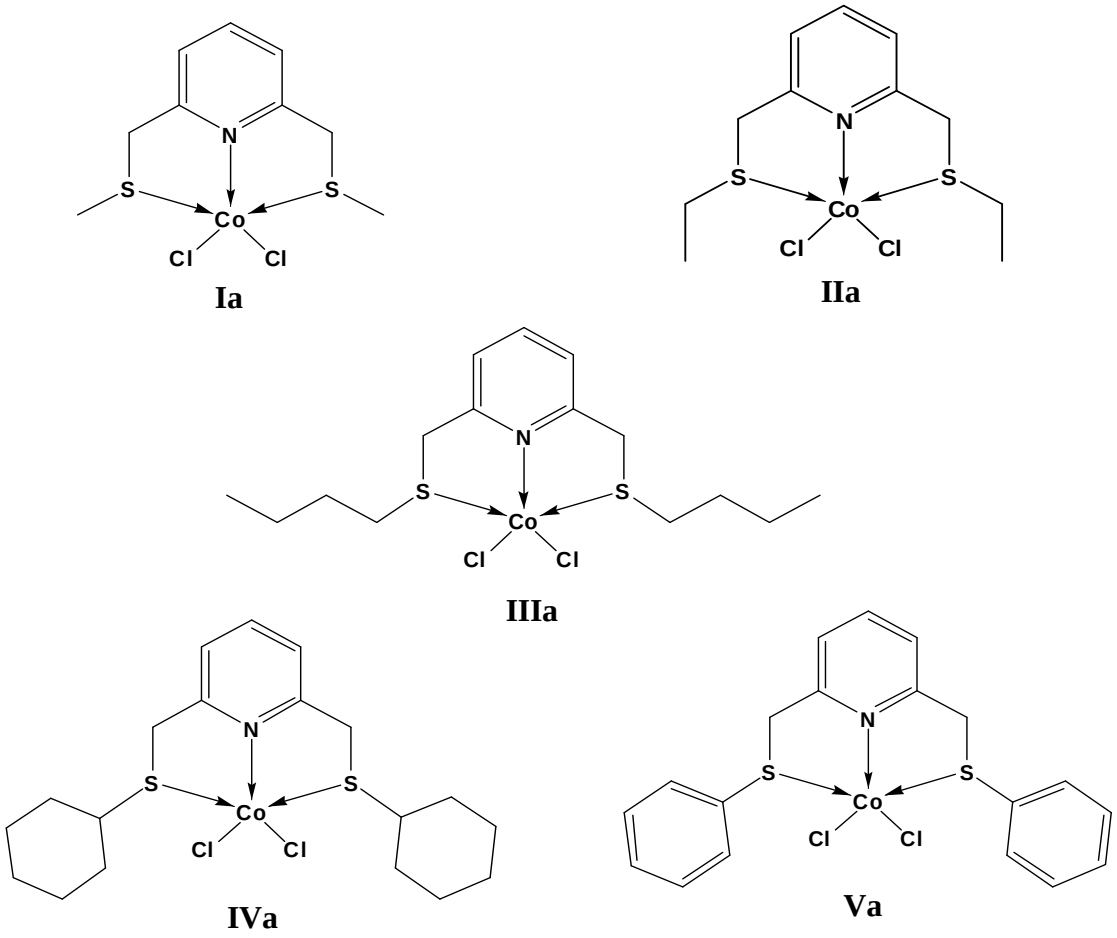

Figure 2.3: Structures of Co complexes containing the pyridine-based SNS ligands.

Table 2.1: Description and yields obtained for each pyridine-based Co complex.

Name	Description	Yield
Ia	Blue microcrystalline solid	0.28 g, 36%
IIa	Bright blue microcrystalline solid	0.07 g, 47%
IIIa	Dark blue crystalline solid	0.65 g, 45%
IVa	Purple powder	0.10 g, 43%
Va	Aqua blue powder	0.17 g, 77%

(b) Amine-based complexes

The structures of complexes **Ib** and **IIb** is given in Fig. 2.4 with the yields and descriptions presented in Table 2.2. Both complexes were prepared in a similar manner under inert atmosphere and the general protocol can be found below. The complex of SNS-decamine was not obtained.

A mixture of the ligand in ethanol (5 ml) was added dropwise to a solution of $CoCl_2.6H_2O$ in ethanol (10 ml) in a 1:1 mole ratio and a colour change from dark blue to indigo-purple was observed. The reaction mixture was allowed to stir for two hours at room temperature after which the solution was concentrated to ~5 ml and the product precipitated out as a lavender coloured solid which was separated via canular filtration.

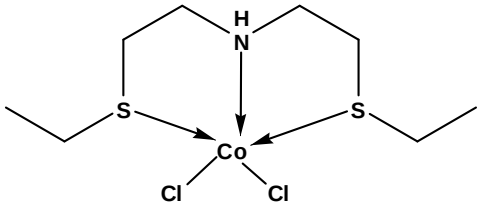

Ib

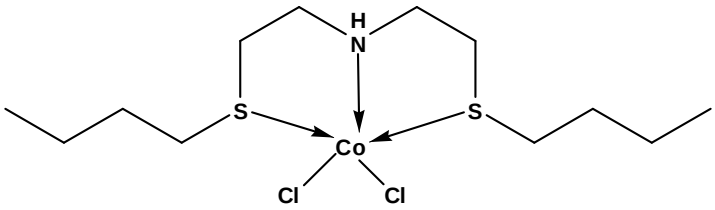

IIb

Figure 2.4: The structures of the Co complexes containing the amine-based SNS ligands.

Table 2.2: Description and yields obtained for each amine-based Co complex.

Name	Description	Yield
Ib	Lavender powder	0.23 g, 66%
IIb	Lavender powder	0.31g, 64%

2.3 Results and discussion

2.3.1 Ligands

The preparation of both the pyridine- and amine-based ligands involved the reaction of the respective thiol with the appropriate precursor to afford the product. For the pyridine-based ligands, the general method was adapted from literature, however a different starting material was used as opposed to the amine-based ligands, where the protocol followed was taken directly from literature without any further modifications.

(a) Pyridine-based ligands

For the preparation of the pyridine-based ligands, the precursor utilised was first synthesised prior to use. In the process, single crystals of the precursor ligand suitable for X-ray crystallography were grown from a THF solution and the crystal structure (Fig. 2.5) was published.[14] The ^{1}H NMR spectrum of this compound is presented in Appendix A2, Fig. A2.25.

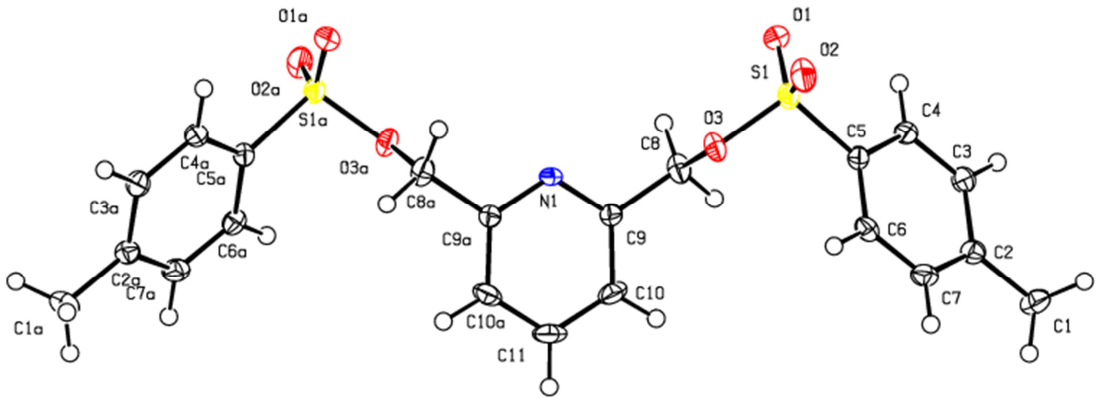

Figure 2.5: ORTEP diagram of the precursor 2,6-pyridine-dimethylene-ditosylate at 50% probability level.

NMR analysis

In this study, NMR was the dominant characterisation technique utilised for the structural elucidation of the ligands. ^{1}H, ^{13}C and ^{13}C DEPT 135 NMR were employed to elucidate the structures and from these experiments important information about the characteristics of each ligand was obtained.

For the pyridine-based ligands, the significant peaks in the ^{1}H NMR spectra were attributed to the backbone, i.e. the aromatic hydrogens, which gave rise to a doublet (7.2 ppm) and a triplet (7.6 ppm) integrating to two hydrogens and one hydrogen respectively, as well as the singlet around 3.8 ppm integrating to four hydrogens, corresponding to the methylene linker between the pyridine ring and the S-donor atoms. A typical example of a ^{1}H NMR spectrum for SNS-mepy is given in Fig. 2.6, while the remaining NMR spectra can be found in Appendix A2 (Figs. A2.1-A2.15).

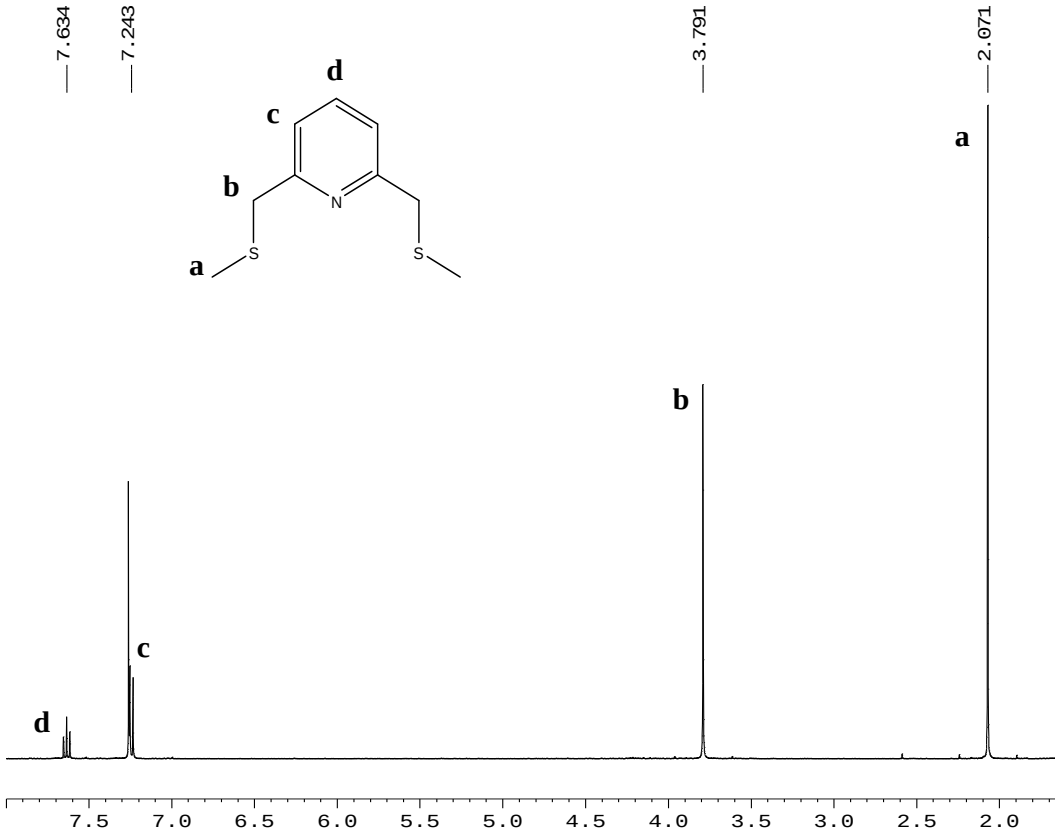

Figure 2.6: ^{1}H NMR spectrum for SNS-mepy.

The ^{13}C NMR spectra showed the signals arising for each carbon atom, which include the characteristic peaks corresponding to the substituents connected to the S-donor atoms and the carbons that make up the pyridine ring. It was observed that the most downfield shifted are the tertiary carbons, typically observed around 158 ppm. The ^{13}C DEPT 135 NMR is an efficient experiment that distinguishes CH_2 (positive) from CH and CH_3 (negative) and an example of this sort of spectrum is presented in Fig. 2.7. For obvious reasons the tertiary carbons on the pyridine ring are not detected since only the carbons bonded to hydrogens give rise to signals in this type of experiment. The ^{13}C DEPT 135 experiment shed more clarity on the structures of the ligands and confirmed the results obtained from the ^{13}C NMR.

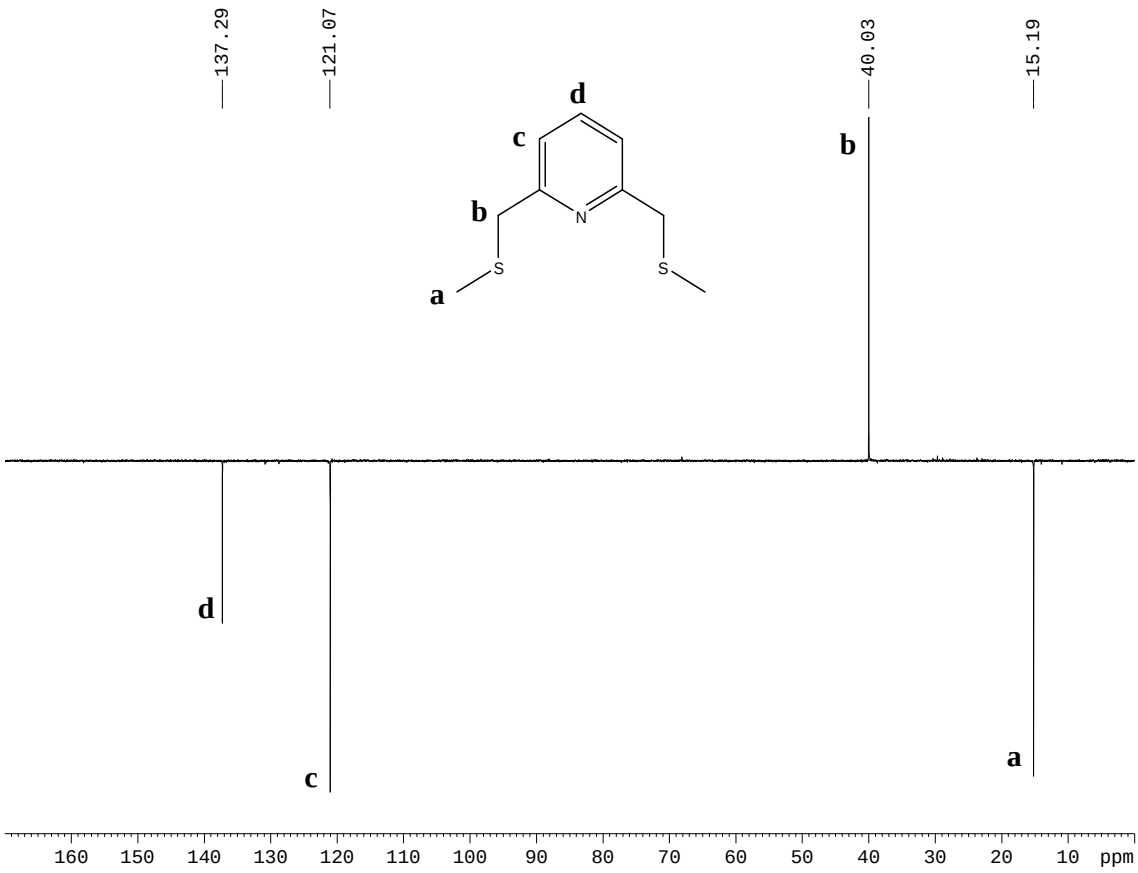

Figure 2.7: ^{13}C DEPT 135 spectrum of SNS-mepy with CH_2 positive and CH, CH_3 negative.

IR analysis

The significant wave numbers for each ligand are presented in Table 2.3 along with the designated functional group to which the signal belongs. The characteristic bands are those that correspond to the C−H aromatic stretch above 3000 cm^{-1}, the C−H alkyl stretch below 3000 cm^{-1} and the C−C aromatic stretches around 1615-1580 cm^{-1}.[15] The C−H rocking is also observed, which is typically in the 750-720 cm^{-1} region,[15] as well as the C−S stretch, that appears around 780-860 cm^{-1} [16].

Table 2.3: IR data obtained for each pyridine-based ligand showing the significant wave numbers in cm^{-1}.

Ligand	**IR ν_{max}/cm^{-1}**					
	C−H (aromatic)[a]	**C−H (alkyl)[b]**	**C−C (aromatic)[c]**	**C-H bend (alkyl)[c]**	**C−H rocking[c]**	**C−S[b]**
SNS-mepy	3058	2966 , 2914, 2856	1589, 1572	1451	747	813
SNS-etpy	3056	2971, 2926, 2869	1590, 1573	1451	747	788
SNS-butpy	3056	2956, 2926, 2871	1589. 1573	1451	747	812
SNS-cypy	3064	2962, 2923	1590, 1571	1480, 1449	737	809
SNS-phpy	3064	2962, 2923	1590, 1571,	1450, 1436	737	809

[a] weak, [b] medium, [c] strong

In addition to the entries in Table 2.3, significant bands at 1480 and 687 cm^{-1} are observed for SNS-phpy which indicates aromatic C−C stretching and C−H out of plane bending respectively, due to the phenyl groups. Bands at 1023 and 993 cm^{-1} are also a result of the cyclohexyl ring vibrations for SNS-cypy. All IR spectra for the pyridine-based ligands are presented in Appendix A2 (Figs. A2.26-A2.30).

MS analysis

The entries in Table 2.4 indicate the m/z ratios obtained for each ligand and were essentially the same as the calculated values represented in parentheses. This was a good indication of successful preparation of the ligands.

Table 2.4: The m/z ratios obtained for each pyridine-based ligand.

Ligand	m/z $[M+H]^+$ (Calculated)
SNS-mepy	200.05 (200.05)
SNS-etpy	228.08 (228.08)
SNS-butpy	284.15 (284.15)
SNS-cypy	336.18 (336.17)
SNS-phpy	324.09 (324.08)

(b) Amine-based ligands

Literature reports[13] have identified the physical appearance of the amine-based ligands as semi-solids (paste), however in these experiments all were obtained as thick oils with the exception of SNS-decamine which, at lower temperatures, appears as a semi-solid (but remains an oil at room temperature).

NMR analysis

The ^{1}H NMR data revealed that the characteristic peaks for the amine-based ligands are the three triplets: 0.9 ppm (6H), 2.6-2.7 ppm (4H) and 2.8 ppm (4H) which correspond to the terminal CH_3, and ethylene linker between the N- and S-donor atoms respectively. However, an anomaly was found with integration for the latter two signals for SNS-decamine and this may be due to the presence of impurities as also observed by the ^{13}C NMR spectrum (Appendix A2, Figs. A2.22, A2.23). The N−H signal was broad and appeared around 1.8 ppm for all three ligands, thus confirming the presence of the N−H functionality. The ^{13}C NMR was straight-forward and the signal that was shifted the most downfield was the carbon closest to the nitrogen, as it is the most deshielded, and these results were also confirmed by

^{13}C DEPT NMR. Overall the NMR spectra showed that the ligands were not completely pure, especially SNS-decamine. However, when comparing the intensities (integrals) of the signals corresponding to the impurities and the ligand, it can be concluded that the impurities are negligible and therefore were ignored. The spectra for the amine-based SNS ligands are presented in Appendix A2, Figs. A2.16-A2.24.

IR analysis

The most important bands in the IR were those corresponding to the N−H stretch (3500-3300 cm^{-1}), the C−H alkyl stretch and bend as well as the C−H rocking vibrations as reported in Table 2.5. However, the IR did not detect the N−H stretch for SNS-decamine or the C−S stretch for all three ligands due to the fact that the former signal is weak and is masked by the intensity of the strong alkyl signal, whereas the latter signals are masked by the strong and broad C−H rocking vibrations. These spectra can be found in Appendix A2, Figs. A2.31-A2.33.

Table 2.5: IR data obtained for each amine-based ligand showing the significant wave numbers in cm^{-1}.

Ligand	**IR ν_{max}/cm^{-1}**				
	N−H stretch[a]	**C−H (alkyl)**	**C-H bend (alkyl)[b]**	**C−H rocking[d]**	**C−S**
SNS-etamine	3288	2962 , 2921, 2864, 2823 [b]	1451	739	N/A
SNS-butamine	3294	2955, 2925, 2872 [c]	1458	741	N/A
SNS-decamine	N/A	2923, 2852 [c]	1460	721	N/A

[a] weak, [b] strong, [c] very strong, [d] broad, strong

MS analysis

The MS results (Table 2.6) reaffirmed that the ligands were successfully synthesised as the m/z values found were identical to the calculated ones.

Table 2.6: The m/z ratios obtained for each amine-based ligand.

Ligand	m/z $[M+H]^+$ (Calculated)
SNS-etamine	194.10 (194.10)
SNS-butamine	250.16 (250.16)
SNS-decamine	418.35 (418.35)

2.3.2 Complexes

After reacting the various SNS ligands with the metal-salt, it is important to characterise the resulting complexes. In order to determine if complexation did occur, a number of characterisation techniques were employed including: IR, elemental analysis, MS, melting point and X-ray crystallography (for selected complexes). Observed changes, such as change in colour that occurred during the course of the reaction, were also important early indicators as to whether the complexation reaction did occur.

The complexes exhibited a range of different colours, especially the pyridine-based complexes, which was the first sign of successful complexation. A noticeable colour change was also observed during the preparation of the amine-based complexes, suggesting that a reaction had taken place leading to product formation. Complexes **Ia-Va** were found to be stable in air, whereas **Ib-IIb** decomposed after prolonged exposure to air and moisture, as a result these complexes were stored in a vacuum desiccator.

When comparing the yields obtained for each complex, it is noted that from the pyridine-based complexes, **Va** was formed in a significantly higher yield than the others (77%). This may have been attributed to the lower solubility of this complex in the ethanol solution and as a result, bulk of it precipitated out as oppose to the other complexes where majority stayed in the solution thus accounting for the lower yields.

Cobalt in the +2 state renders a high spin complex which is paramagnetic and as a result NMR studies could not be carried out for all the complexes in this study as no signals were observed when the samples were analysed. Hence, other available techniques, including IR, elemental analysis and single crystal X-ray diffraction were employed for complex characterisation and molecular structure determination.

IR analysis

The IR data obtained for each ligand was compared to those of the corresponding complex with the aim of observing any changes or shifts in band positions. Significant shifts were identified as presented in Table 2.7. In the aromatic C−H region, shifts were detected from higher to lower wavenumbers for the majority of the complexes thereby indicating weakening of the C−H bonds in the pyridine ring after complexation. This is expected since, upon forming a coordinative bond with the metal, some of the electron density is transferred to the metal−N bond thus drawing electron density away from the pyridine ring, causing the energy of the vibrations of the C−H bonds within the ring to decrease, giving rise to signals at lower wavenumbers. For complex **IVa** a drastic shift from 2962 to 2928 cm^{-1} is noted in the alkyl C−H region as compared to the other complexes and this suggests that C−H bonds in the cyclohexyl ring become significantly weaker after complexation. This is accompanied by a shift from 1480 to 1455 cm^{-1} for the C−H bend. In this case, electron density is lost within the cyclohexyl ring when the metal−S bond is formed resulting in a decrease of the energy of the alkyl bonds. Complexes **IIa-Va** showed a shift from lower to higher wavenumbers in the C−C aromatic region which suggest that these bonds are strengthened.

Reports have shown that the C−S stretch for coordinated S-donor atoms appears in the 690-720 cm^{-1} region and are weaker as opposed to the bands of the uncoordinated ligand, which occur at 780-860 cm^{-1} and are markedly stronger.[16] Observations of the the C−S stretch in **Ia-Va** confirms this trend immediately, which is a clear indication of S coordination to Co.

Complex **Ib** did not exhibit a distinct shift in the N−H region, however for complex **IIb** a shift from 3294 to 3219 cm^{-1} was detected which implies that this bond got weaker after complexation. Other shifts in the C−H region were observed and although the C−S stretching vibrations were masked in the ligand spectra, the signals are noted in the spectra of the complexes further confirming successful complexation.

Table 2.7: The shifts observed in the IR from the ligands to the complexes.

	IR ν_{max}/cm^{-1}			
	C−H (aromatic)[a]	**C−H (alkyl)[b]**	**C−C (aromatic)[c]**	**C−S[a]**
SNS-mepy	3058	2966	1572	812
Ia	3053	2999	1567	716
SNS-etpy	3056	2971	1590	788
IIa	3031	2965	1601	711
SNS-butpy	3056	2956	1589	812
IIIa	3067	2958	1598	723
SNS-cypy	3064	2962	1590	809
IVa	3056	2928	1599	725
SNS-phpy	3064	2962	1590	809
Va	3059	2953	1602	720
	IR ν_{max}/cm^{-1}			
	N−H stretch[a]	**C−H (alkyl)[b]**	**C-H bend (alkyl)[b]**	**C−S[a]**
SNS-etamine	3228	2864	1458	N/A
Ib	3228	2870	1465	694
SNS-butamine	3294	2872	1458	N/A
IIb	3219	2867	1464	744

[a] weak(for the co-ordinated S), [b] medium, [c] strong

Elemental analysis

Elemental analysis for each complex showed that the experimental value was in acceptable range to that of the theoretically calculated value represented in parentheses, as shown in Table 2.8. This not only supported that the complexation was successful, but also that the

complexes were of high purity, thus implying that the impurities present from the ligand remained in solution when the complex precipitated out during the reaction.

Table 2.8: The elemental analysis obtained for each complex.

Complex	%C	%H	%N
		(Calculated)	
Ia	32.4 (32.8)	4.4 (4.0)	4.0 (4.3)
IIa	37.3 (37.0)	5.2 (4.8)	3.85 (3.9)
IIIa	45.0 (44.5)	6.6 (6.8)	3.4 (3.1)
IVa	48.6 (49.0)	6.8 (6.3)	2.8 (3.0)
Va	50.1 (50.3)	4.3 (3.8)	3.0 (3.1)
Ib	29.6 (29.7)	6.3 (5.9)	4.2 (4.3)
IIb	37.9 (38.0)	7.6 (7.2)	3.7 (3.7)

MS results

In theory, the MS results of the complexes should represent the total mass corresponding to the complex in question. However, when the mass spectra for the SNS complexes were obtained, only the mass of the ligand was observed. Since other characterisation techniques have unequivocally pointed to the successful isolation of the complexes, it was then safe to assume that the ligand may have detached from the metal during the ionisation process which would explain why only the ligand mass was identified. To confirm this theory, when a crystalline sample that had already been successfully characterised by X-ray crystallography as the complex was investigated by MS, a similar result was obtained thus confirming the assumption.

Melting point

The melting point range of a complex can give an indication of how pure it is. Impurities usually lower the melting point and cause a wider melting range when compared to purer compounds which have higher and sharper melting points. Table 2.9 presents the melting

point obtained for each complex. It can be seen that complex **Ia** shows two thermal events, and this is because the complex exists as a dimer in the solid state, which was later confirmed by X-ray crystallography. The first point is attributed to the transition from the dimer to the monomer and the second the actual melting of the monomer. As the chain length of the substituent increases on the S-donor atoms from complex **Ia** to **IIIa** and **Ib** to **IIb**, there is a noticeable decrease in the melting point. This is because as the chain length is increased, there is greater degrees of free rotation and hence greater tendency towards disorder which result in lower melting points.[17] The relatively sharp melting points indicated that all the complexes were of high purity.

Table 2.9: The melting point ranges obtained for each complex.

Complex	Melting point/°C
Ia	176-177, 196-197
IIa	164-165
IIIa	107-108
IVa	142-143
Va	211-213
Ib	171-172
IIb	144-145

2.4 Attempted complexation to iron

Iron was the first metal chosen for investigation in this research since it is a biomimetic, economical and a relatively non-toxic metal. No information was discovered in the literature on Fe-based SNS complexes which increased our interest and served as the inspiration for further exploration into potential Fe(SNS) catalysts. Several attempts were made at complexing both types of SNS ligands to Fe to no avail. Varying Fe precursors were employed along with different reaction conditions, however none were successful.

The first attempt was the use of iron pentacarbonyl, $Fe(CO)_5$, for which no reaction occurred because the carbonyl groups were bonded too strongly to Fe and the SNS ligand was not a strong enough donor to induce CO dissociation.[18] It was then decided to use a precursor that can be easily replaced by the SNS ligand e.g. $Fe(CO)_2(C_7H_8)$.[19] This is because firstly cycloheptatriene (C_7H_8) is more likely to be replaced by the SNS ligand than the carbonyls and the reaction can be monitored by IR due to the presence of the other two carbonyl groups. However, the attempted synthesis of this complex was unsuccessful. Therefore, $Fe(PPh_3)_2Cl_3$[20] was chosen and successfully synthesised, but when reacted with the ligand, no reaction occurred. The other routes chosen involved simple addition reactions using well known Fe salts like $FeCl_2$ and $FeCl_3$ and still no successful reactions were obtained even with $Fe(acac)_3$.

After all these attempts, Co was chosen as the metal for complexation. It is probable that Fe being a harder metal, when compared to Co, is unlikely to interact with softer donors like sulfur, a potential reason why thus far, to the best of our knowledge, no information is available in the literature on the successful complexation of an SNS ligand to Fe. Further investigations in the future would involve increasing the hardness of the sulfur donors by adding electron donating groups which would potentially increase the electron density at the S-donor atoms, as well as decreasing the hardness of Fe by adding electron withdrawing ligands that would decrease the electron density at the metal centre. This could possibly encourage the interaction of Fe with the SNS ligand.

2.5 Summary

The successful preparations of seven novel cobalt-based SNS complexes have been achieved. All complexes were NMR inactive, due to their paramagnetic properties, and hence were characterised by IR, elemental analysis and melting point. In certain cases, crystals suitable for X-ray crystallographic studies were obtained and these will be discussed in the following chapter. Several attempts to complex SNS-decamine to cobalt and the other ligands to iron were unsuccessful.

References

(1) Bai, S.-Q.; Koh, L. L.; Hor, T. S. A. *Inorganic Chemistry* **2009**, *48*, 1207.

(2) Canovese, L.; Visentin, F.; Chessa, G.; Uguagliati, P.; Santo, C.; Bandoli, G.; Maini, L. *Organometallics* **2003**, *22*, 3230.

(3) Teixidor, F.; Sanchez-Castello, G.; Lucena, N.; Escriche, L.; Kivekas, R.; Sundberg, M.; Casabo, J. *Inorganic Chemistry* **1991**, *30*, 4931.

(4) Klerman, Y.; Ben-Ari, E.; Diskin-Posner, Y.; Leitus, G.; Shimon, L. J. W.; Ben-David, Y.; Milstein, D. *Dalton Transactions* **2008**, 3226.

(5) Bassetti, M.; Capone, A.; Salamone, M. *Organometallics* **2003**, *23*, 247.

(6) Koizumi, T.-a.; Teratani, T.; Okamoto, K.; Yamamoto, T.; Shimoi, Y.; Kanbara, T. *Inorganica Chimica Acta*, *363*, 2474.

(7) (a) Canovese, L.; Chessa, G.; Marangoni, G.; Pitteri, B.; Uguagliati, P.; Visentin, F. *Inorganica Chimica Acta* **1991**, *186*, 79. (b) Canovese, L.; Visentin, F.; Chessa, G.; Uguagliati, P.; Bandoli, G. *Organometallics* **2000**, *19*, 1461. (c) Teixidor, F.; Escriche, L.; Casabo, J.; Molins, E.; Miravitlles, C. *Inorganic Chemistry* **1986**, *25*, 4060.

(8) Liu, F.; Anis, R.; Hwang, E.; Ovalle, R.; Varela-Ramírez, A.; Aguilera, R. J.; Contel, M. *Molecules* **2011**,*16*, 6701.

(9) McGuinness, D. S.; Wasserscheid, P.; Keim, W.; Morgan, D.; Dixon, J. T.; Bollmann, A.; Maumela, H.; Hess, F.; Englert, U. *Journal of the American Chemical Society* **2003**, *125*, 5272.

(10) Bluhm, M. E.; Walter, O.; Döring, M. *Journal of Organometallic Chemistry* **2005**, *690*, 713.

(11) Reger, D. L.; Semeniuc, R. F.; Smith, M. D. *Crystal Growth & Design* **2005**, *5*, 1181.

(12) Temple, C. N.; Gambarotta, S.; Korobkov, I.; Duchateau, R. *Organometallics* **2007**, *26*, 4598.

(13) Konrad, M.; Meyer, F.; Heinze, K.; Zsolnai, L. *Journal of the Chemical Society, Dalton Transactions* **1998**, 199.

(14) Komarsamy, L.; Bala, M. D.; Friedrich, H. B.; Omondi, B. *Acta Crystallographica* **2011**, *E67*, 302.

(15) Coates, J. In *Encyclopedia of Analytical Chemistry*; Meyers, R. A., Ed.; John Wiley and Sons Ltd, Chichester, 2000.

(16) Allen, E. A.; Johnson, N. P.; Rosevear, D. T.; Wilkinson, W. *Journal of the Chemical Society* **1971**, *A*, 2141.

(17) Brown, R. J. C.; Brown, R. F. C. *Journal of Chemical Education* **2000**, *77*, 724.

(18) Downing, S. P.; Hanton, M. J.; Slawin, A. M. Z.; Tooze, R. P. *Organometallics* **2009**, *28*, 2417.

(19) Abel, E. W.; Bennett, M. A.; Burton, R.; Wilkinson, G. **1958**, 4559.

(20) Walker, J. D.; Poli, R. *Inorganic Chemistry* **1989**, *28*, 1793.

CHAPTER THREE

Crystal structures of the metal complexes

3.1 General

X-ray crystallography is a method that is used to determine the crystal structure of a particular compound. It is a characterisation technique that provides unequivocal structural information regarding the compound in question. Important features like bond angles and lengths can be determined, the geometry as well as the angles of the planes can be obtained. This type of technique is crucial, especially when complexes are difficult to characterise by other techniques due to the intricacy or complexity of the structure or inability to analyse the sample by more direct methods (e.g. NMR in this case).

The growing of single crystals suitable for analysis by X-ray crystallography is a challenging task. Not all compounds are able to crystallise, some molecules are incapable of organising in an ordered manner and exist as non-crystalline solids or oils, while some crystallise but not in a quality good enough for diffraction studies. It is therefore essential that available techniques are utilised for growing suitable crystals, such as layering, slow diffusion or slow evaporation. All these methods were employed for the growth of single crystals for complexes **Ia**, **IIa** and **IIIa**.

3.2 Crystal structures

Intensity data were collected on a Bruker APEX II CCD area detector diffractometer with graphite monochromated Mo K_α radiation (50kV, 30mA) using the APEX 2 data collection software.[1] The collection method involved ω-scans of width 0.5° and 512x512 bit data frames. Data reduction was carried out using the program *SAINT+* and face indexed absorption corrections were made using *XPREP*.[2]

The crystal structure was solved by direct methods using *SHELXTL*.[3] Non-hydrogen atoms were first refined isotropically, followed by anisotropic refinement by full matrix least-

squares calculations based on F^2 using *SHELXTL*. Hydrogen atoms were first located in the difference map, then positioned geometrically and allowed to ride on their respective parent atoms. Diagrams and publication material were generated using SHELXTL, PLATON[4] and ORTEP-3.[5] Selected crystallographic and structure refinement data are presented in Table 3.1. The supporting information for each crystal structure is presented in Appendix A3.

Table 3.1: Selected crystallographic and structure refinement data for Complexes Ia-IIIa.

	Ia	**IIa**	**IIIa**
Empirical formula	$C_{18}H_{26}Cl_4Co_2N_2S_4$	$C_{11}H_{17}Cl_2CoNS_2$	$C_{15}H_{25}Cl_2CoNS_2$
Formula weight	658.31	357.21	413.31
Temperature (K)	173(2)	173(2)	173(2)
Wavelength (Å)	0.71073	0.71073	0.71073
Crystal system	Triclinic	Monoclinic	Monoclinic
Space group	P-1	Cc	C2/c
Unit cell dimensions			
a (Å)	7.5980(2)	24.9529(9)	34.5930(9)
b (Å)	8.4802(2)	7.9877(3)	7.6101(2)
c (Å)	10.5727(3)	16.5411(6)	15.5012(4)
α (°)	80.6050(10)	90	90
β (°)	83.4030(10)	112.111(2)	99.7340(10)
γ (°)	69.8060(10)	90	90
Volume ($Å^3$)	629.51(3)	3054.44(19)	4022.04(18)
Z	1	8	8
Density (calculated) (Mg/m^3)	1.736	1.554	1.365
Absorption coefficient (mm^{-1})	2.085	1.725	1.320
F(000)	334	1464	1720
Crystal size (mm^3)	0.53 x 0.27 x 0.21	0.15 x 0.10 x 0.04	0.434 x 0.371 x 0.20
Theta range for data collection (°)	1.96 to 28.00.	1.76 to 27.00	2.39 to 26.00°.
Index ranges	-8<=h<=10, -11<=k<=11, -13<=l<=13	-31<=h<=31, -10<=k<=10, -21<=l<=21	-42<=h<=40, -9<=k<=9, -18<=l<=18
Reflections collected	10432	13589	16675
Independent reflections	3035 [R(int) = 0.0390]	6536 [R(int) = 0.0597]	3959 [R(int) = 0.0368]

Completeness to theta = 28.00° (%)	100.0	100.0	99.9
Absorption correction	Integration	Integration	Integration
Max. and min. transmission	0.6686 and 0.4046	0.9364 and 0.8378	0.7913 and 0.6118
Refinement method	Full-matrix least-squares on F^2	Full-matrix least-squares on F^2	Full-matrix least-squares on F^2
Data / restraints / parameters	3035 / 0 / 138	6536 / 2 / 311	3959 / 48 / 168
Goodness-of-fit on F^2	1.124	1.039	1.079
Final R indices [I>2sigma(I)]	R1 = 0.0310, wR2 = 0.0773	R1 = 0.0551, wR2 = 0.1268	R1 = 0.0679, wR2 = 0.2236
R indices (all data)	R1 = 0.0366, wR2 = 0.0797	R1 = 0.0850, wR2 = 0.1756	R1 = 0.0829, wR2 = 0.2428
Largest diff. peak and hole ($e.Å^{-3}$)	0.405 and -1.467	0.544 and -0.420	0.852 and -0.792

3.2.1 Complex Ia

Dark blue, cubic single crystals of **Ia** were obtained over a period of two weeks from a concentrated acetonitrile solution layered with diethyl ether. An ORTEP representation of **Ia** is shown in Fig 3.1.

The ORTEP diagram reveals octahedral geometry around each Co metal in a highly symmetrical dimeric molecular unit of complex **Ia**. The molecular structure also shows that the SNS ligand coordinates in a terdentate fashion to the metal centre via two S- and one N-donor atoms. The other three sites are occupied by a terminal and two bridging chloride groups, where a bridging chloride of each identical unit creates the linkage between the dinuclear units. Therefore, the complex exists as a dimer of two six coordinate Co centres related through a centre of inversion. This correlates with the melting point herein reported for this complex where two “melting” stages were observed. The pyridyl group and the chlorides occupy the equatorial positions, while the sulfur atoms reside in the two axial positions.

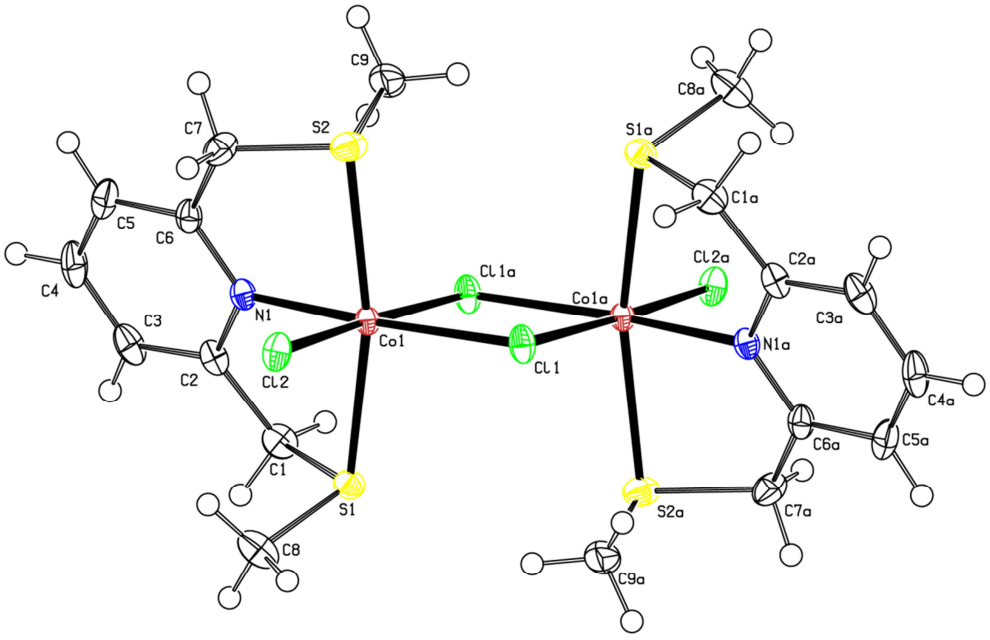

Figure 3.1: ORTEP diagram of complex **Ia** shown at the 50% probability level.

The closest example found in literature is a Cr(SNS) complex that exhibits a similar dinuclear molecular frame.[6] Relatively weak metal-metal interactions were observed between the two octahedral centres of **Ia** separated through space by a Co---Co distance of 3.684 Å, which is longer than similar distances in square planar SNS metal complexes bearing *t*-butyl groups on the S-donor atoms having dimeric centres with separations of 3.223 and 3.255 Å for Ir---Ir and Ru---Ru[7] centres respectively. Table 3.2 presents selected bond lengths and angles for complex **Ia**.

Slight geometric differences are observed for related bond lengths in the molecular specie of **Ia**. For instance, when comparing the bond lengths for the bridging chlorine atoms Cl(1)-Co(1) and Co(1)-Cl(1)1a it is noted that the former is slightly shorter than the latter with the values being 2.4133 and 2.5274 Å respectively. The N(1)-Co(1) bond length of 2.1131 Å and the S(1)-Co(1) and S(2)-Co(1) bond lengths of 2.4980 and 2.4889 Å, respectively, deviate slightly from the literature[6] where 2.070 Å were reported for the N-Cr bond length, while 2.453 and 2.446 Å were reported for the S(1)-Cr and S(2)-Cr bonds respectively.

Table 3.2: Selected bond lengths (Å) and angles (°) for complex **Ia**.

Bond lengths/Å	
N(1)-Co(1)	2.1131(17)
S(1)-Co(1)	2.4980(5)
S(2)-Co(1)	2.4889(6)
Cl(1)-Co(1)	2.4133(6)
Cl(2)-Co(1)	2.3618(5)
Co(1)-Cl(1)1a	2.5274(5)
Bond angles/°	
N(1)-Co(1)-Cl(2)	92.96(5)
N(1)-Co(1)-Cl(1)	171.92(5)
Cl(2)-Co(1)-Cl(1)	95.052(19)
N(1)-Co(1)-S(2)	81.33(5)
Cl(2)-Co(1)-S(2)	87.82(2)
Cl(1)-Co(1)-S(2)	97.98(2)
N(1)-Co(1)-S(1)	81.84(5)
Cl(2)-Co(1)-S(1)	96.342(19)
Cl(1)-Co(1)-S(1)	98.22(2)
S(2)-Co(1)-S(1)	162.85(2)
N(1)-Co(1)-Cl(1)1a	88.41(5)
Cl(2)-Co(1)-Cl(1)1a	177.78(2)
Cl(1)-Co(1)-Cl(1)1a	83.610(19)
S(2)-Co(1)-Cl(1)1a	94.11(2)
S(1)-Co(1)-Cl(1)1a	82.124(18)

1a = -x, -y, -z

The bite angle, which is usually defined by the ligand-metal-ligand angle,[8] is represented by the S(1)-Co(1)-S(2) angle and is quite obtuse at 162.85(2)° for **Ia**, implying a very open coordination sphere around Co. This bite angle value is quite comparable to the values displayed by similar SNS containing complexes, such as S(1)-Cr-S(2) of 164.04(11)°.[6]

The pyridyl plane defined by N(1), C(2), C(3), C(4), C(5), C(6) and the metal enclosing SNS plane defined by S(1), N(1), S(2), Co(1) dissect each other at an acute angle of 15.91°, slightly out of planarity, implying that the Co-SNS complex is not an entirely flat and planar molecule. This molecular non-planarity may be attributed to the slight twisting of the methyl

'arms' (atoms C1 and C7) linking the pyridine ring to each of the S-donor atoms with the atoms positioned on either side of the S-N-S-Co plane deviating from it by 0.750 Å and 0.744 Å respectively. A similar scenario is observed with the Ru(SNS) complex reported by Viñas *et al*. where there is a deviation from the S-N-S-Ru plane by ±0.66-0.91 Å.[9]

3.2.2 Complex IIa

Blue, plate-like single crystals were deposited after several weeks from a concentrated ethanolic solution of **IIa**. An ORTEP representation of complex **IIa** is shown in Fig 3.2.

Complex **IIa**, crystallises in the monoclinic *Cc* space group with four twins (independent molecules A & B, Fig. 3.2) in the asymmetric unit cell. The Co atom in each molecule exists as a five coordinate centre stabilised by the SNS ligand and two terminal chlorine atoms. The geometry in **IIa** differs significantly from **Ia** as a result of simply extending the S-atom substituent from methyl to the ethyl group. The bulkier and electron richer ethyl group may be partly responsible for the propensity of **IIa** to exist as a five coordinate monomer, while **Ia** easily dimerises in an octahedral fashion.

The frameworks of molecules A and B are essentially identical and therefore the crystal structure of **IIa** will be discussed with reference to the parameters for molecule A only. Selected bond lengths and angles are presented in Table 3.3. From a comparison of the bond lengths in Table 3.2 and 3.3 it is noted that the N(1)-Co(1) bond is shorter than that of **Ia** [2.048(7) Å vs. 2.1131(17) Å], while the S(1)-Co(1) and S(2)-Co(1) bond lengths are longer, thus indicating that the Co-N bond is stronger and the Co-S bonds are weaker in **IIa**.

A distorted trigonal bipyramidal geometry is observed for **IIa** due to the narrower bite angle of S(2)-Co(1)-S(1). The equatorial positions are occupied by the two chloride groups and the N-donor atom, while the axial positions are taken up by the two S-donor atoms. Literature revealed a complex of Zn(SNS)[10] with a similar conformation to **IIa** that showed a S(1)-Zn-S(2) bite angle of 157.0 Å, which is slightly more acute than observed for **IIa** (161.90(8)°).

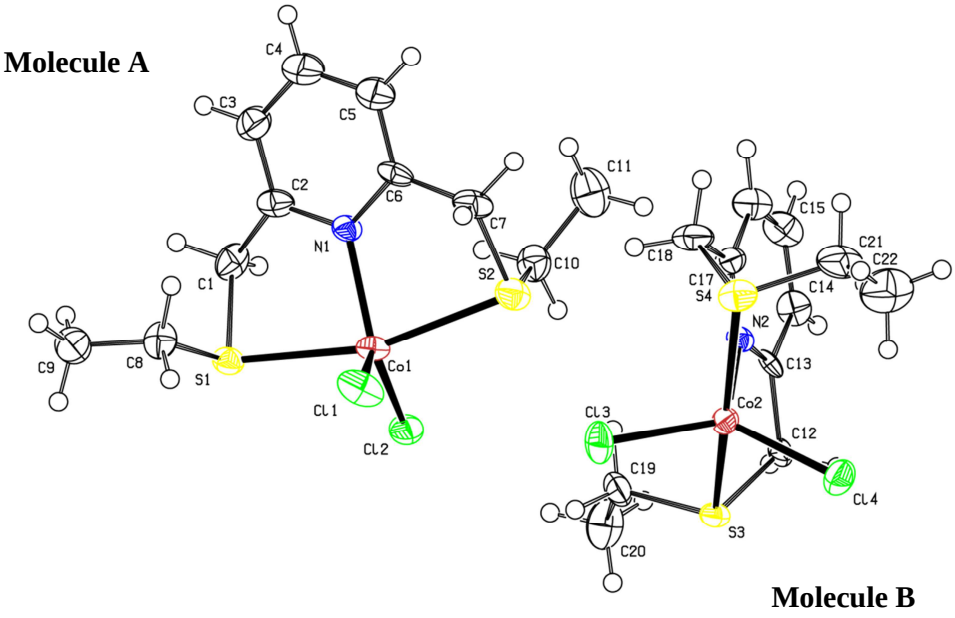

Figure 3.2: ORTEP diagram of complex **IIa** at the 50% probability level showing two crystallographically independent molecules (A & B) in the asymmetric unit cell.

Table 3.3: Selected bond lengths (Å) and angles (°) for complex **IIa**.

Bond lengths/Å	
N(1)-Co(1)	2.048(7)
S(1)-Co(1)	2.521(2)
S(2)-Co(1)	2.518(3)
Cl(1)-Co(1)	2.268(3)
Cl(2)-Co(1)	2.274(2)
Bond angles/°	
N(1)-Co(1)-Cl(2)	126.6(2)
N(1)-Co(1)-Cl(1)	108.5(2)
Cl(2)-Co(1)-Cl(1)	124.87(10)
N(1)-Co(1)-S(2)	81.5(2)
Cl(2)-Co(1)-S(2)	95.17(9)
Cl(1)-Co(1)-S(2)	93.72(9)
N(1)-Co(1)-S(1)	82.3(2)
Cl(2)-Co(1)-S(1)	88.09(8)
Cl(1)-Co(1)-S(1)	99.01(10)
S(2)-Co(1)-S(1)	161.90(8)

The planes defined by N(1), C(2), C(3), C(4), C(5), C(6) and S(1), N(1), S(2), Co(1) dissect each other at an angle of 17.25° and just as with complex **Ia**, the substituent 'arms' are situated on opposite sides of the S-N-S-Co plane such that C(1) and C(7) deviate from the plane by 0.903 and 0.774 Å respectively.

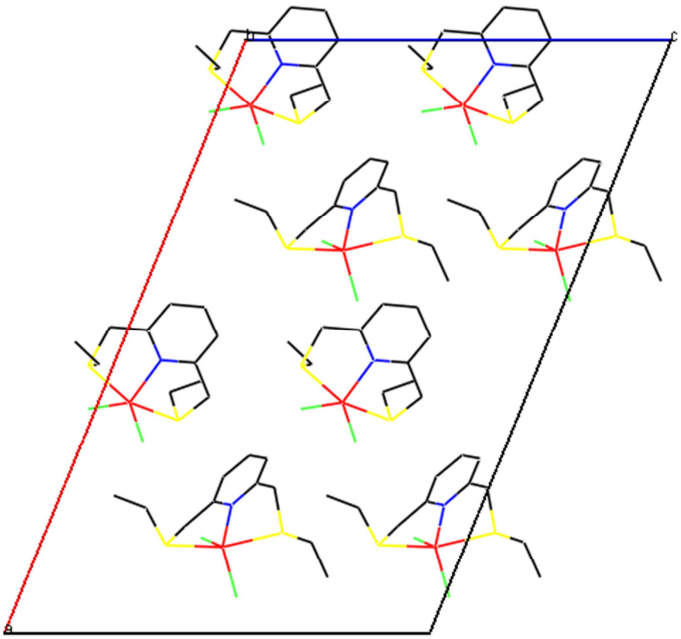

Figure 3.3: Wireframe representation of the crystal packing of complex **IIa** with the hydrogen atoms omitted for clarity.

An observation of the crystal packing of **IIa** revealed an ordered arrangement of the crystal units containing the A and B molecules in alternating rows (Fig. 3.3), as a result a higher melting point was obtained (164-165°) compared to complex **IIIa** (107-108°). Primarily the more order displayed by the crystal unit, the more energy is required to cause a phase transition.[11]

3.2.3 Complex IIIa

Single crystals suitable for X-ray diffraction were obtained in a similar manner to **IIa**. The crystals of **IIIa** are dark blue to indigo in colour and have a plate-like appearance.

From Fig. 3.4 it is observed that the butyl groups on the S-donor atoms are highly disordered.

The larger ball-like ellipsoids indicate the disorder in the carbon positions of the butyl groups which have occupancy over two positions, however only one conformation is presented for clarity. The disorder arises due to atomic agitation of the free end of the butyl chain about the anchored S-C bond.

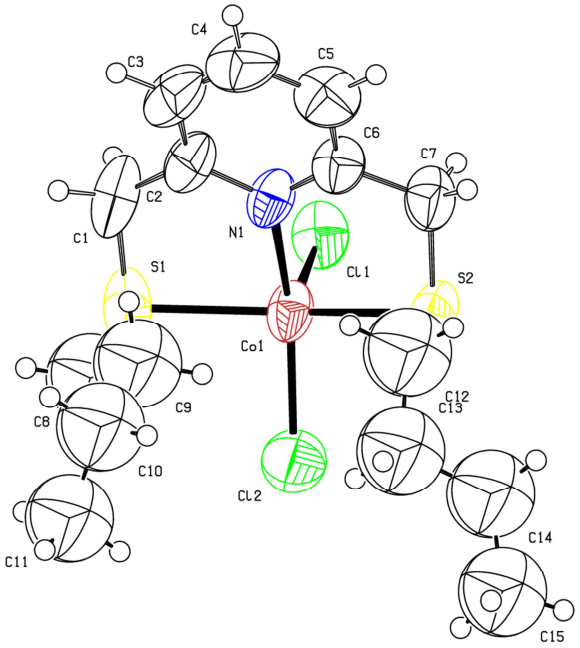

Figure 3.4: ORTEP diagram of complex **IIIa** at the 50% probability level showing one conformation of the disordered butyl group.

It is noted that **IIIa** also exists as a monomer, much like **IIa**, thus confirming the increase in steric bulk theory behind the preferential monomeric states of these two complexes. Selected bond lengths and angles are presented in Table 3.4. Distorted trigonal bipyramidal geometry is displayed by **IIIa**, with the pyridyl moiety and the two chloride groups occupying the equatorial positions, while the two S-donor atoms take up the axial positions. The N(1)-Co(1), S(1)-Co(1) and S(2)-Co(1) bond lengths for **IIIa** are very similar to **Ia**, but a noticeably more acute bite angle of 152.55(7)° is observed in comparison to **Ia** and **IIa**.

Table 3.4: Selected bond lengths (Å) and angles (°) for complex **IIIa**.

Bond lengths/Å	
N(1)-Co(1)	2.133(3)
S(1)-Co(1)	2.4496(15)
S(2)-Co(1)	2.4604(14)
Cl(1)-Co(1)	2.2787(15)
Cl(2)-Co(1)	2.2734(17)
Bond angles/°	
N(1)-Co(1)-Cl(2)	150.53(11)
N(1)-Co(1)-Cl(1)	96.96(10)
Cl(2)-Co(1)-Cl(1)	112.51(6)
N(1)-Co(1)-S(2)	80.80(10)
Cl(2)-Co(1)-S(2)	95.17(9)
Cl(1)-Co(1)-S(2)	93.72(9)
N(1)-Co(1)-S(1)	82.07(11)
Cl(2)-Co(1)-S(1)	92.56(7)
Cl(1)-Co(1)-S(1)	99.01(10)
S(2)-Co(1)-S(1)	152.55(7)

The pyridine ring is rotated slightly such that C(2) and C(6) reside on the S-N-S-Co plane, whereas C(3), C(4) and C(5) deviate from the plane by 0.383, 0.485 and 0.313 Å respectively, causing the angle of dissection between it and the pyridyl plane [N(1), C(2), C(3), C(4), C(5)] to be 11.81°. Unlike in the case of complexes **Ia** and **IIa**, the substituent 'arms' C(1) and C(7) are positioned on the same side of the S-N-S-Co plane, deviating by just 0.155 and 0.287 Å respectively.

The steric bulk and disorder brought about by the butyl groups is responsible for the relatively low melting point of 107-108 °C for **IIIa** compared to the other complexes reported herein.[11] The packing in a crystal of **IIIa** is represented in Fig. 3.5 showing the low symmetry of the compound. Neighbouring molecules are arranged in a repeating 'head-to-head' followed by a 'tail-to-tail' orientation related through a 2-fold rotation axis and a 2-fold centre of rotation.

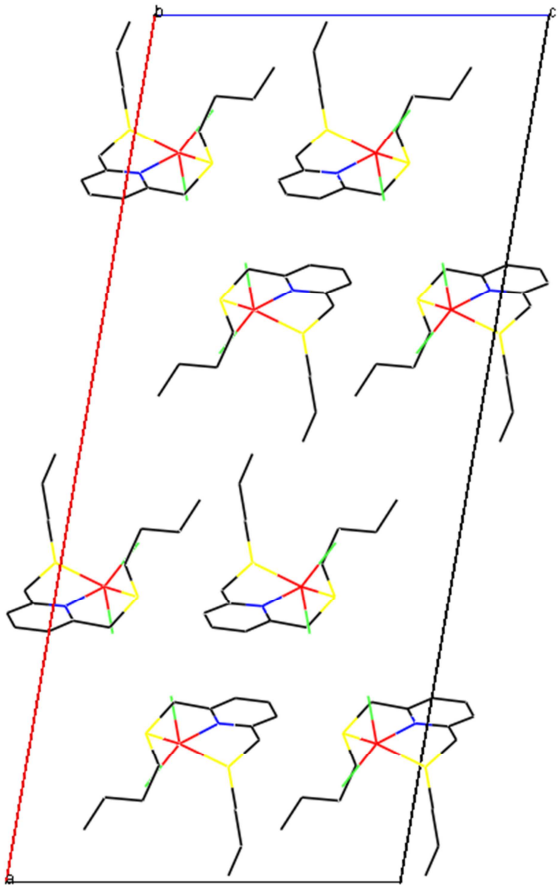

Figure 3.5: Wire frame representation of the crystal packing of complex **IIIa** with the hydrogen atoms omitted for clarity.

References

(1) Bruker (2005a). APEX2. Version 2009.1-0. Bruker AXS Inc., Madison, Wisconsin, USA.

(2) Bruker (2005b). SAINT+. Version 7.60A. (includes XPREP and SADABS) Bruker AXS Inc., Madison, Wisconsin, USA.

(3) Bruker (1999). SHELXTL. Version 5.1. (includes XS, XL, XP, XSHELL) Bruker AXS Inc., Madison, Wisconsin, USA.

(4) Spek, A. L. *Journal of Applied Crystallography* **2003**, *36*, 7.

(5) Farrugia, L. J. *Journal of Applied Crystallography* **1997**, *30*, 565.

(6) Temple, C. N.; Gambarotta, S.; Korobkov, I.; Duchateau, R. *Organometallics* **2007**, *26*, 4598.

(7) Klerman, Y.; Ben-Ari, E.; Diskin-Posner, Y.; Leitus, G.; Shimon, L. J. W.; Ben-David, Y.; Milstein, D. *Dalton Transactions* **2008**, 3226.

(8) van Zeist, W. J.; Bickelhaupt, F. M. *Dalton Transactions* **2011**, *40*, 3028.

(9) Viñas, C.; Anglès, P.; Sánchez, G.; Lucena, N.; Teixidor, F.; Escriche, L.; Casabó, J.; Piniella, J. F.; Alvarez-Larena, A.; Kivekäs, R.; Sillanpää, R. *Inorganic Chemistry* **1998**, *37*, 701.

(10) Teixidor, F.; Escriche, L.; Casabo, J.; Molins, E.; Miravitlles, C. *Inorganic Chemistry* **1986**, *25*, 4060.

(11) Brown, R. J. C.; Brown, R. F. C. *Journal of Chemical Education* **2000**, *77*, 724.

CHAPTER FOUR

Paraffin oxidation studies

4.1 Introduction

This chapter details the application of the prepared cobalt complexes for the oxidative functionalisation of saturated hydrocarbons, also known as paraffins. The impetus for this type of catalysis has been described in detail in Chapter one, where the importance of paraffin oxidation was outlined and specified examples were mentioned (Section 1.2). To the best of our knowledge there are no reported pincer complexes of cobalt applied for paraffin oxidation. The novelty of this section of the project is further highlighted since all the complexes are novel.

Literature has revealed Co(III) alkyl peroxo complexes applied for hydrocarbon oxidation. The complexes yielded ROO• and RO• radicals, upon heating in solution, which are the active species involved in oxidizing the hydrocarbon substrate.[1] Other examples of Co catalysed hydrocarbon oxidation include fluorous biphasic systems incorporating the macrocycle tetraazacyclotetradecane.[2]

The formation of oxygenates from saturated hydrocarbons by the use of peroxide species is a process that commonly occurs via free radical mechanisms, although there are other pathways followed which were outlined in Section 1.3 of this report. In addition to molecular oxygen, various other oxidants have been applied for this process, including hydrogen peroxide, alkyl hydroperoxides and peroxy acids.[3] Biological systems have been the inspiration for the development of synthetic catalysts in the application of hydrocarbon oxidation (Section 1.1) and these systems most often involve radical pathways as well.[4]

The chemistry behind the radical mechanisms can be explained as follows:

1. Essentially, the metal catalyses the decomposition of the peroxide species which in turn generates oxy radicals (Scheme 4.1, eq 1).

2. The oxy radicals then abstract a hydrogen from the alkane substrate creating an alkyl radical R• (Scheme 4.1, eq 2).

3. The alkyl radical then reacts with O_2 to produce the peroxo radicals, ROO• (Scheme 4.1, eq 3).

4. The peroxo radicals transforms into alkyl hydroperoxide (Scheme 4.1, eq 4) which, during the course of the reaction, decomposes to yield the alcohol and ketone products.[3,5,6]

Generally, the aldehydes and carboxylic acids are formed from the further oxidation of the terminal alcohol and, quite often, the alcohols are further oxidised to produce more ketones, a process known as deep oxidation.

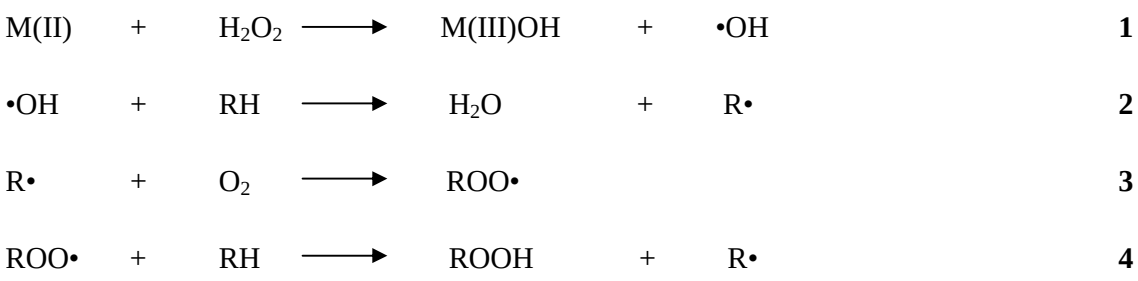

Scheme 4.1: The radical pathways followed during paraffin oxidation.

In the case of *tert*-butyl hydroperoxide as the oxidant, instead of •OH radicals being produced in the initiation step, *t*-BuOO• and *t*-BuO• radicals are formed. Work by Chavez *et al*. has shown that the *t*-BuOO• radicals do not possess sufficient radical strength to abstract a hydrogen from the hydrocarbon substrate as does *t*-BuO•, hence it decomposes to yield the reactive *t*-BuO•.[1b]

Attempts at the functionalisation of paraffins have highlighted some of the problems associated with these efforts. The production of terminal products is usually very rare and if there are any, the conversions are relatively low and this is generally associated with the strength of the terminal C−H bond (being the strongest bond on the hydrocarbon chain it is difficult to cleave).[7] Further recognition is placed on the inert nature of C−H bonds in saturated hydrocarbons which lead to overall relatively low conversions in the catalytic process.[8]

Another common problem faced is the low selectivity of oxidative catalysis and hence the preferential oxidation of one carbon atom in a paraffin chain is a difficult task to fulfil.[9] The regioselectivity (the preferential functionalisation of one carbon position over another in a hydrocarbon chain) and the stereoselectvity (the favoured formation of one stereoisomer over another) can be improved if the reactive metal centres are coordinated to bulky substituents.[9]

In this study, the prepared Co complexes **Ia-IIb** were applied for the oxidation of *n*-octane to oxygenates using two types of peroxides: hydrogen peroxide (H_2O_2) and *tert*-butyl hydroperoxide (*t*-BuOOH). Experimental conditions were also optimised in favour of substrate conversion and product selectivity.

4.2 Materials and instrumentation

All catalytic reactions were carried out under inert nitrogen atmosphere to avoid air oxidation and the solvent was deoxygenated by passing a stream of nitrogen through it. The oxidants H_2O_2 (30%) and *t*-BuOOH (70%) were purchased from DLD Scientific and Sigma-Aldrich respectively, and used as supplied. The reagents utilised for the calibration of the GC: 1-octanol (99%), 2-octanol (97%), 3-octanol (98%), 4-octanone (99%), octanal (99%) and octanoic acid (99%) were obtained from Sigma-Aldrich, 2-octanone (98%), 3-octanone (97%), 4-octanol (98%) and *n*-octane (99%) were sourced from Fluka, and pentanoic acid (98%) from Merck. The solvent acetonitrile (99%) was obtained from Sigma-Aldrich.

A Perkin Elmer Auto System GC was employed which was integrated with a Flame Ionisation Detector (FID) for the analysis of the products. Table 4.1 depicts the column specifications and GC parameters. The duration of each GC run was 34 min, excluding the oven cooling time.

Table 4.1: Column specifications and GC parameters used for the analysis of the oxygenated products.

Column	**Pona 50 m X 0.20 mm X 0.5 µm**			
Injector temperature	240 °C			
Detector temperature	260 °C			
Split	On flow rate: 123 ml min^{-1}			
Attenuation	4			
Range	1			
	Oven temperature			
Initial temperature/°C	**Ramp one/°C/min**	**Temperature two/°C**	**Ramp two/°C/min**	**Temperature three/°C**
50	2	90	15	200

4.3 General experimental procedure

The paraffin oxidation studies were carried out using *n*-octane as the substrate with pentanoic acid as the internal standard. The catalytic reactions were performed under a nitrogen atmosphere in a 50 ml two-neck pear shaped flask equipped with a condenser. The reaction mixture consisted of 5 ml degassed acetonitrile (solvent), the respective peroxide (H_2O_2 or *t*-BuOOH), *n*-octane and the respective catalyst (3 mg). The reaction mixture was stirred in an oil bath at the optimum temperature and after the time period, an aliquot of the sample was removed with a Pasteur pipette and filtered through a cotton wool plug, after which 0.5 µL of the aliquot was injected into the GC for analysis and quantification.

The masses and volumes of the components of the reaction mixture (Appendix A4, Table A4.1) were dependent on the specific catalyst, however the catalyst loading was kept constant at 1 mol%, i.e. a catalyst to substrate mole ratio of 1:100. Also the *n*-octane to oxidant ratio was varied to obtain the optimum ratio. All the reactions carried out in this section were checked for reproducibility and data reported are averages of at least two reproduced results that were within acceptable experimental limits of error.

The studies carried out with 1-octanol and 2-octanol were performed in a similar manner as that of *n*-octane, with a catalyst to substrate to oxidant mole ratio of 1:100:2000 and a time period of five hours using catalyst **Ib** as a representative system (Appendix A4, Table A4.2).

4.4 Results and discussion

4.4.1 The oxidation of *n*-octane using H_2O_2

The oxidation of *n*-octane was investigated with H_2O_2 as the oxidant, since it is a common oxygen source used in research and industry for hydrocarbon oxidations.[6,8,10,11] Among other oxidants, H_2O_2 has both economical and environmental benefits[12] and hence its use is advantageous. Acetonitrile was chosen as the solvent due to its ability to dissolve the catalyst and its relatively high polarity,[12] which allows miscibility with water that makes up 70% of the H_2O_2 solution or 30% of the *t*-BuOOH solution.

Blank reactions were carried out at the optimum reaction temperature of 80 °C to determine if any thermally initiated oxidation may occur without any catalyst. No conversion was observed at substrate to oxidant mole ratios of 1:2, 1:3, 1:6 and 1:9.

However, there was no observable reactivity displayed by the catalysts in the presence of this oxidant and this lead to the belief that this may be a harsh oxidant which resulted in the decomposition of the catalyst, rather than promoting oxidation of the substrate.

4.4.2 The oxidation of *n*-octane using *t*-BuOOH

The oxidant *t*-BuOOH is known to be a milder oxidant than H_2O_2[9] and is therefore anticipated not to deactivate or decompose the catalyst as quickly. Furthermore, this oxidant is known to be more effective than H_2O_2 in some cases.[13] To determine if *t*-BuOOH was active in the absence of the catalyst, blank reactions were carried out at varying *n*-octane to oxidant mole ratios and a total conversion of 1% of *n*-octane to oxygenates was found for all ratios, with the exception of 1:30 where a total conversion of 2% was recorded (Fig. 4.2). As expected, no conversion was observed for blank runs that contained the catalyst in the absence of the oxidant.

4.4.2.1 Optimisation of reaction conditions: time and *t*-BuOOH ratio

To determine the optimum reaction time, the reaction mixture was refluxed for a period of 24, 48, and 72 hours to observe its time dependence. The results of this study are presented in Fig. 4.1. Complexes **Ia** and **Va** were used to carry out this study as representative catalysts for the pyridine-based complexes. It can be concluded from Fig. 4.1 that 48 hours is the optimum time for oxidation of *n*-octane. Moreover, it is also noted that the amine-based complex **IIb** showed a drop in the conversion after 24 hours. The noticeable difference in the stability of the amine-based complex, as compared to the pyridine-based ones, under the oxidation conditions may be attributed to the higher relative stability (due to electron delocalisation) of the pyridine ring to oxidative attack. From these results, it was concluded that 48 hours and 24 hours were the optimum reaction times for the pyridine- and amine-based catalysts respectively.

Reactions at varying *n*-octane to *t*-BuOOH mole ratios were then carried out to determine the most productive optimum ratio. Substrate to oxidant mole ratios of 1:3, 1:6, 1:9, 1:12, 1:20, 1:30 and 1:40 were investigated using complex **Va** as a representative catalyst. It was discovered that as the amount of oxidant is increased, the total conversion of *n*-octane also increases, but drops drastically for ratios of 1:30 and 1:40 (Fig. 4.2). This suggests that at 1:30 and 1:40, the amount of the oxidant *t*-BuOOH is too high in the reaction vessel, which possibly increased the rate of attack on the catalyst, thus accounting for the sudden decrease in conversion. Since 1:20 was the optimum ratio, as it yielded the highest conversion, all the remaining catalytic testing was carried out at this mole ratio.

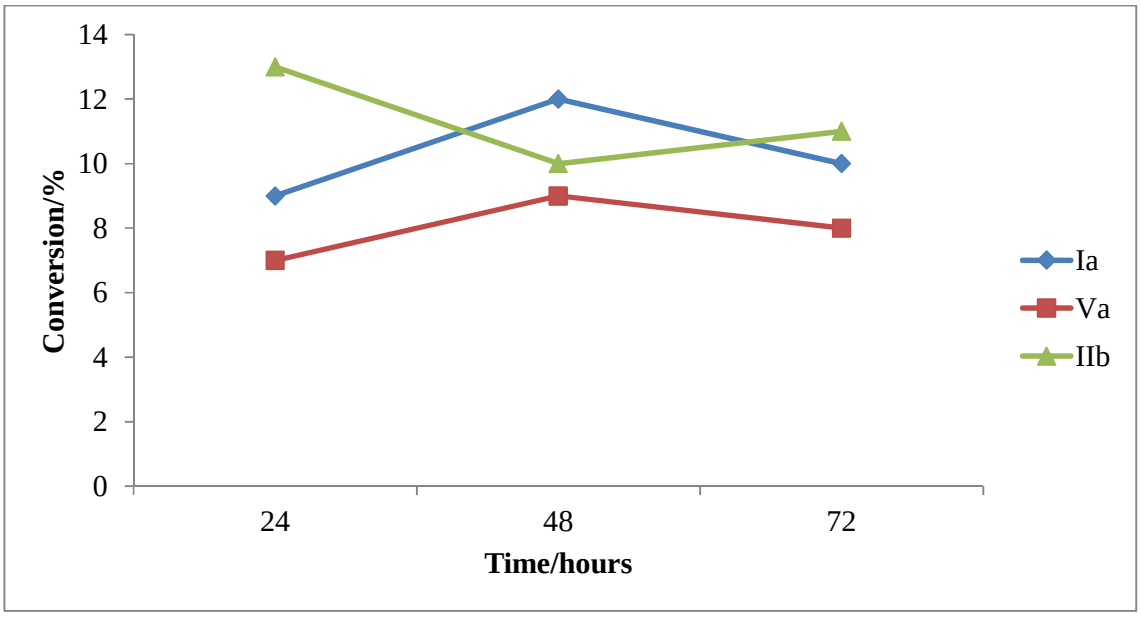

Figure 4.1: The total conversion of *n*-octane over a period of 72 hours for **Ia**, **Va** and **IIb**.

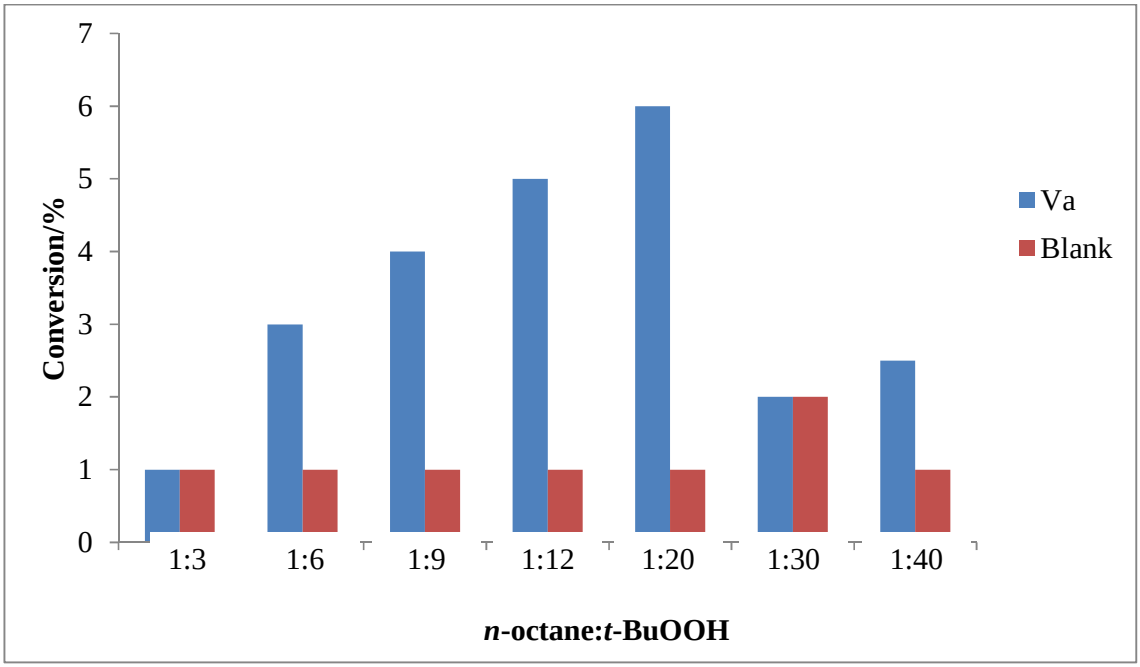

Figure 4.2: The total conversion of *n*-octane at varying mole ratios of *n*-octane to *t*-BuOOH for **Va** relative to the blank.

4.4.2.2 Testing of complexes Ia-IIb at the optimum conditions

The oxidation of *n*-octane in the presence of *t*-BuOOH with catalysts **Ia-IIb** at the optimum conditions produced a mixture of isomeric ketones and alcohols that were oxygenated at carbon positions 1, 2, 3 and 4, as well as other terminal products like octanal and octanoic acid. Figs. 4.3 and 4.4 shows, respectively, the total conversion and selectivity profiles obtained for all seven catalysts in this study. The total conversion was calculated as total moles of product/initial moles of substrate while the selectivity was calculated as moles of each product/total moles of product and both were expressed as a percentage. The individual selectivity profiles for each catalyst are presented in Appendix A4, Figs. A4.1-A4.7.

This information suggests that amongst the pyridine-based catalysts, **Ia** was the most active, showing the highest total conversion of *n*-octane (12%). Theoretically, this was expected considering the fact that this catalyst had the least sterically hindered active site due to the relatively small methylene groups bonded to the S-donor atoms, which allowed for greater access to the metal centre and consequently enhanced catalytic activity. As the chain length of the R groups on the S-donor atoms increased, the conversion started to decrease indicating that the active site became further hindered, thus lowering activity.

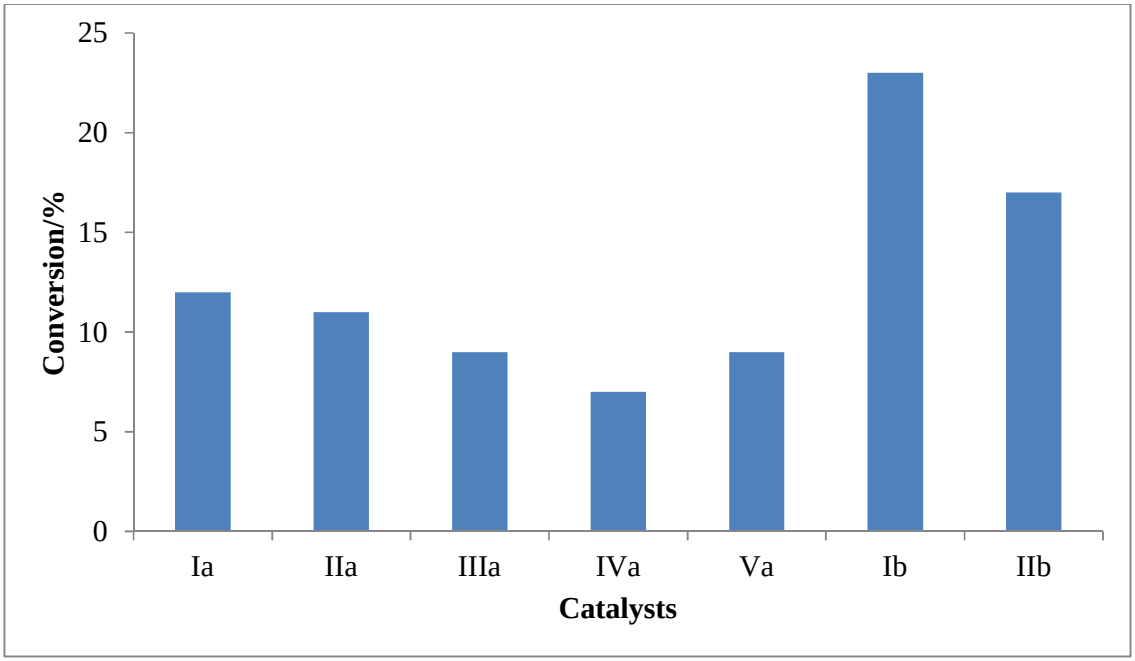

Figure 4.3: The total conversion of *n*-octane at the optimum conditions for catalysts **Ia-IIb**.

Furthermore, the substituents become more electron donating as the chain length increases, which suggests that an increase in electron density may result in decreased conversion of the substrate. Supporting this, when focusing on **IVa** and **Va**, it is noted that the cyclohexyl groups on the S-donor atoms are more electron donating than the phenyl groups. Since the trend observed is an inverse relationship between the conversion and electronic behaviour of the substituents, there is a noticeable increase in conversion from **IVa** to **Va**.

The amine-based catalysts displayed a significantly higher catalytic activity with conversions of 23% and 17% for **Ib** and **IIb** respectively. This implies that the flexibility of the backbone of the catalyst greatly affects the catalytic activity. The main reason for the decrease in conversion from **Ib** to **IIb** can be attributed to the electronic factor once again. Overall **Ib** displayed the most promising catalytic activity.

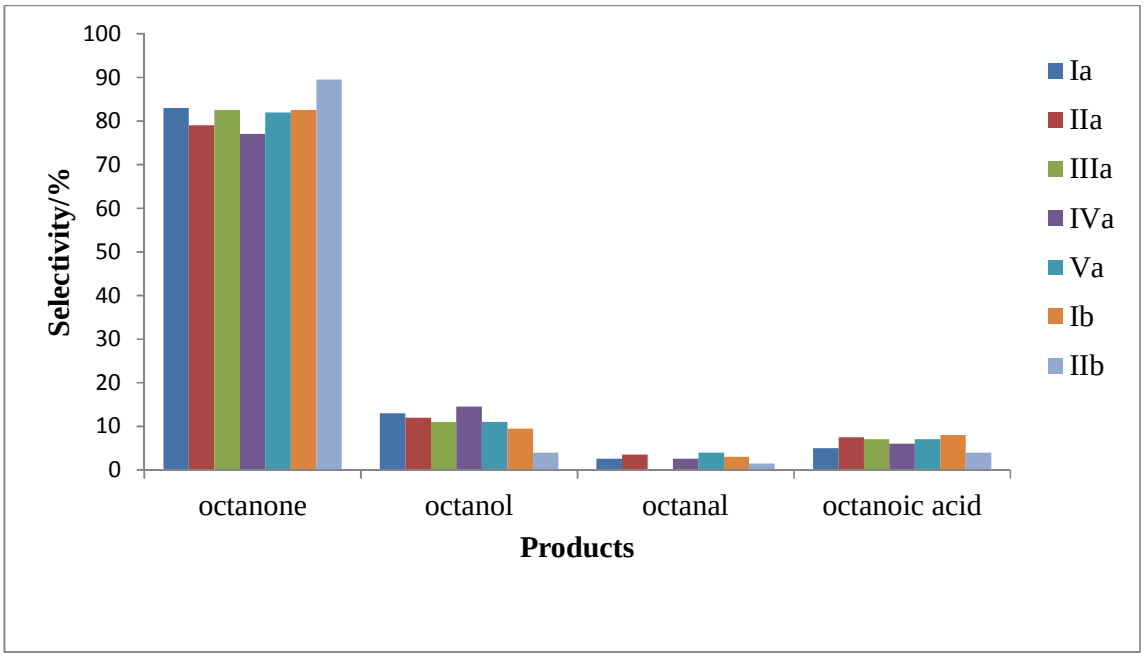

Figure 4.4: The selectivity profile showing the product distribution for catalysts **Ia-IIb**.

Taking product selectivity into consideration, it was found that the ketones were the dominant products overall, with selectivities of up to ca. 90% as an improvement over the previously reported selectivity of ca. 80%.[9] However, catalyst **IIb** was the most selective towards the ketone products. The general trend of selectivity to each ketone displayed by the catalysts was: 2-octanone > 3-octanone > 4-octanone, with 2-octanone significantly predominating.

Catalyst **IVa** showed the highest selectivity to the alcohol products and consequently the lowest selectivity to the ketone products. This can be attributed to the steric control offered by the bulky cyclohexyl groups.[9] As mentioned previously, under oxidative conditions there is tendency for the alcohol products to be further oxidised to form the corresponding ketone (shown later in Fig. 4.8). Hence, to prevent this from occurring, the selectivity of the catalyst may be enhanced by coordinating ligands to the metal centre that contain bulky substituents[9] and this steric effect was observed with **IVa**.

When the selectivity to terminal products were calculated (Table 4.2) no coherent trend was observed. The order of selectivity towards the terminal products is: **IIb** < **Ia** < **IIIa** < **IVa** < **Ib** < **Va** < **IIa**. Catalyst **IIa** and **Va** were the most selective to the terminal products (which include 1-octanol, octanal and octanoic acid) and this suggests that relative to the other catalysts, these two catalysts have the ability to more easily attack the terminal carbon atom.

Table 4.2: The selectivity to the terminal products calculated for catalysts **Ia**-**IIb**.

Catalysts	Selectivity/%
Ia	10
IIa	15
IIIa	10
IVa	11
Va	14
Ib	13
IIb	7

The plot of selectivity to each terminal or C(1) product is presented in Fig. 4.5. Overall, octanoic acid is the dominant product formed for all catalysts. The 1-octanol to octanal to octanoic acid ratio remains consistent at 1:1:2 for catalysts **Ia-Va**, with the exception of **IIIa**, and 1:1.5:4 for **Ib-IIb**. This information suggests that octanoic acid is a product of over oxidation and that the sequence of product formation is in the order:[14]

1-octanol ⟶ octanal ⟶ octanoic acid

In order to confirm whether indeed the higher oxygenates were products of sequential oxidation, a study of the oxidation of 1-octanol using **Ib** as the representative catalyst was conducted. Fig. 4.6 clearly shows that the first product formed was the aldehyde from which octanoic acid was obtained. As the selectivity of octanal decreases, that of octanoic acid increases over a period of five hours, thus confirming that 1-octanol was oxidised to octanal, which was subsequently oxidised to produce the octanoic acid. Furthermore, it was observed that complete oxidation of the 1-octanol and octanal did not occur since the total conversion of 1-octanol was only 17% and after the five hour time period octanal was still present in the reaction mixture. This was also the observation for catalysts **Ia**-**IIb**, with the exception of **IIIa** where no octanal was present (Fig. 4.5) thus implying that in this one anomaly there was complete oxidation of octanal to octanoic acid.

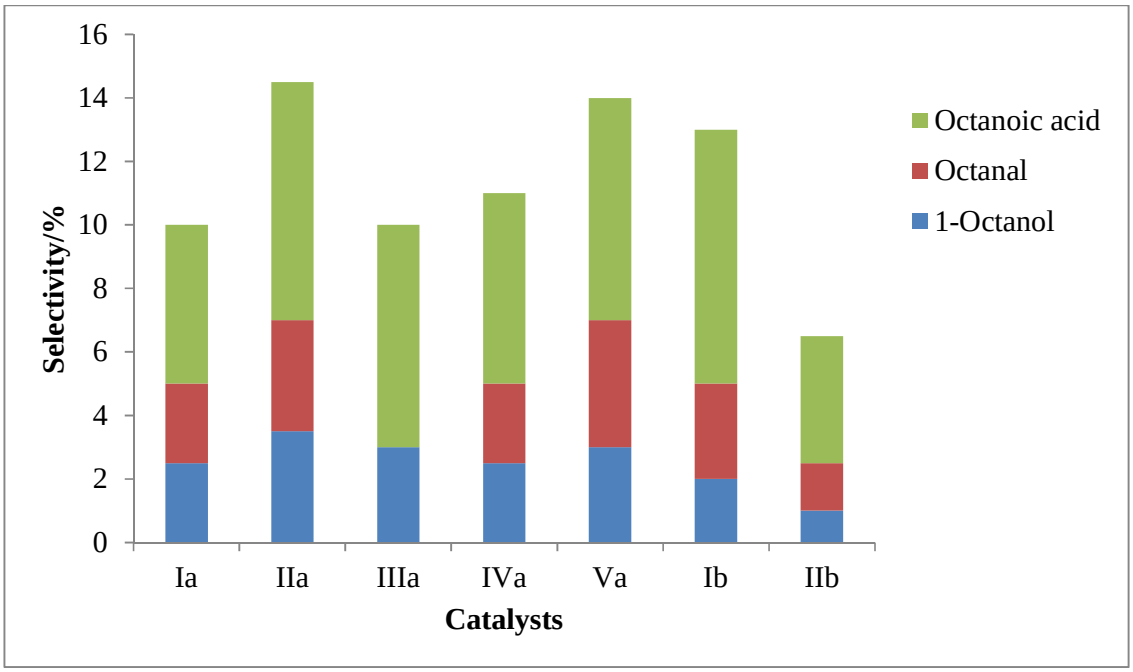

Figure 4.5: The selectivity to C(1) products for catalysts **Ia**-**IIb**.

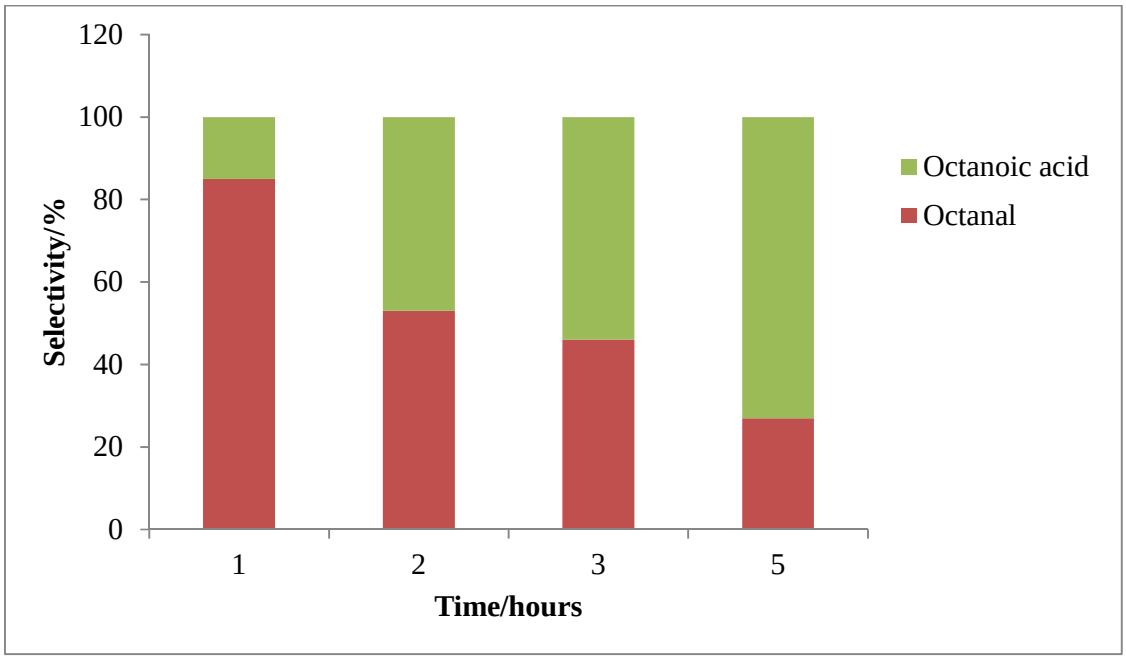

Figure 4.6: The selectivity of octanal and octanoic acid in the oxidation of 1-octanol with **Ib**.

The selectivity of the alcohol and ketone products at position C(2) on the hydrocarbon chain (Fig. 4.7) revealed that the ketones were formed in large excess to the alcohols as a result of over oxidation.

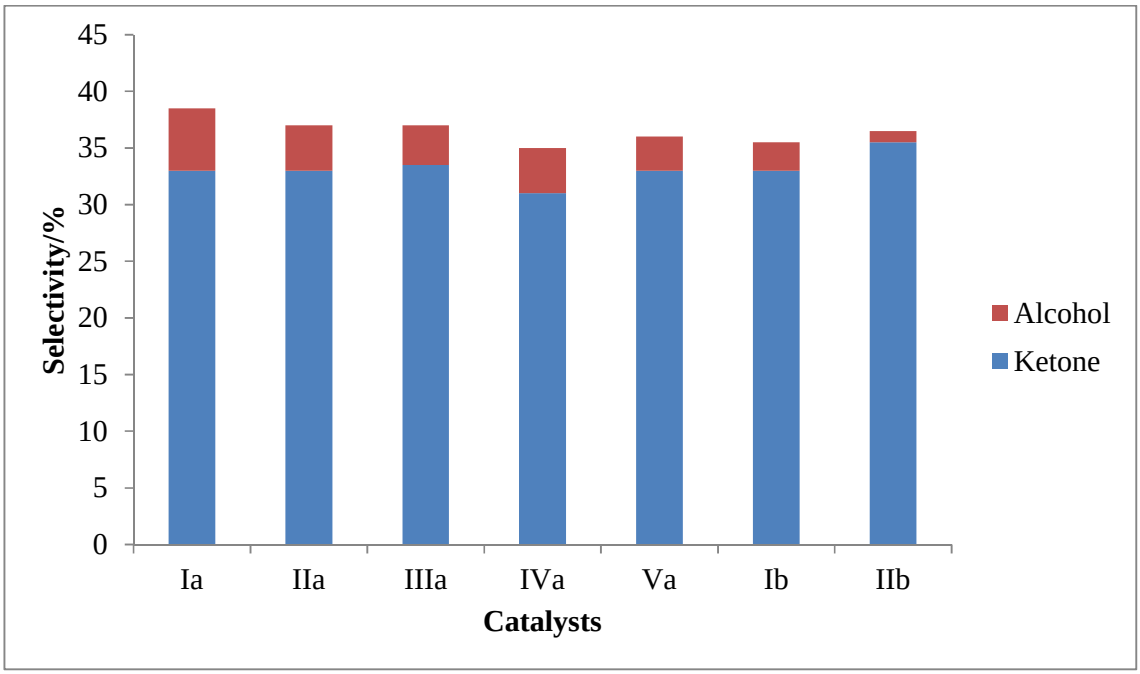

Figure 4.7: The selectivity to C(2) products for catalysts **Ia-IIb**.

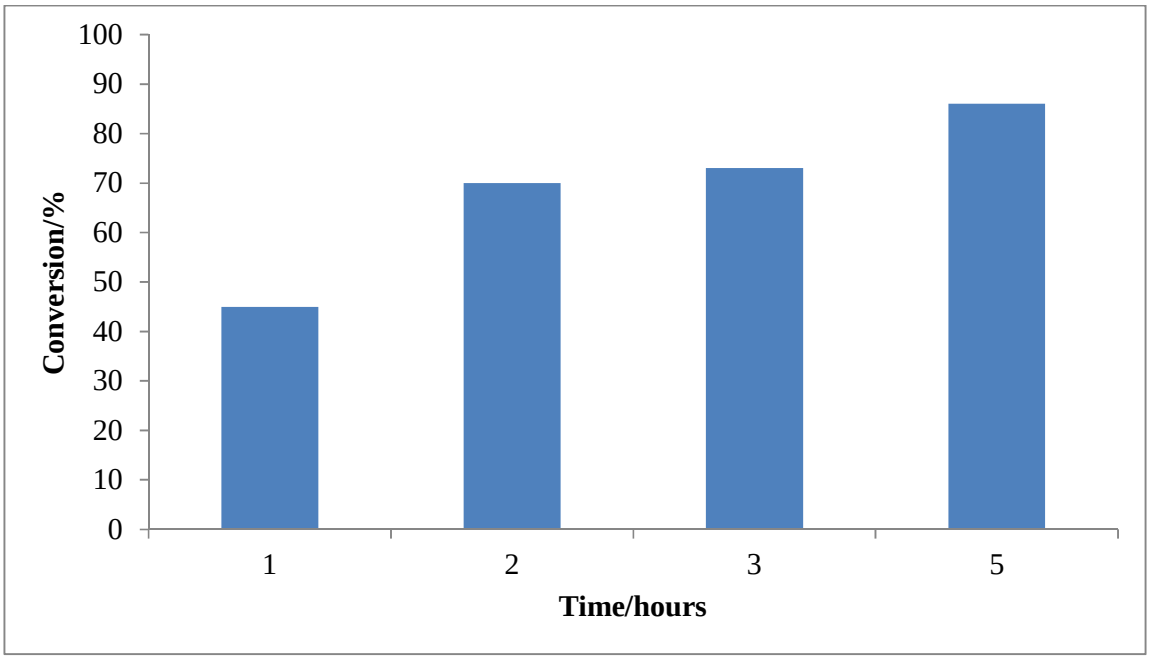

Figure 4.8: The conversion of 2-octanol to 2-octanone over a five hour time period using **Ib**.

In order to gain some insight on the rates of the secondary oxidation of alcohol to ketone reactions, a study of the oxidation of 2-octanol was carried out with **Ib** as the representative catalyst over a period of five hours (Fig. 4.8). The trend observed was time dependent production of 2-octanone, i.e. as the time increases, the production of 2-octanone from 2-octanol increased. At five hours, the total conversion of 2-octanol was found to be 86%, hence indicating that the oxidation of octanols (including 1-octanol) proceeds quite early and relatively quickly in the oxidation process. Moreover, since the optimum conversion was achieved over a period of 24 and 48 hours for the catalytic systems investigated in this study, over oxidation is inevitable.

Considering the selectivity to the C(3) products (Fig. 4.9), it is seen that no alcohol was found for catalysts **IIa**, **IVa**, **Va** and **IIb** which implies that complete oxidation of 3-octanol to 3-octanone had occurred. Catalyst **Ia** showed the highest selectivity to 3-octanol (5%) followed by **Ib** (3%) with the lowest observed for **IIIa** (1%). Here also, no observable trend can be attributed to catalyst structure.

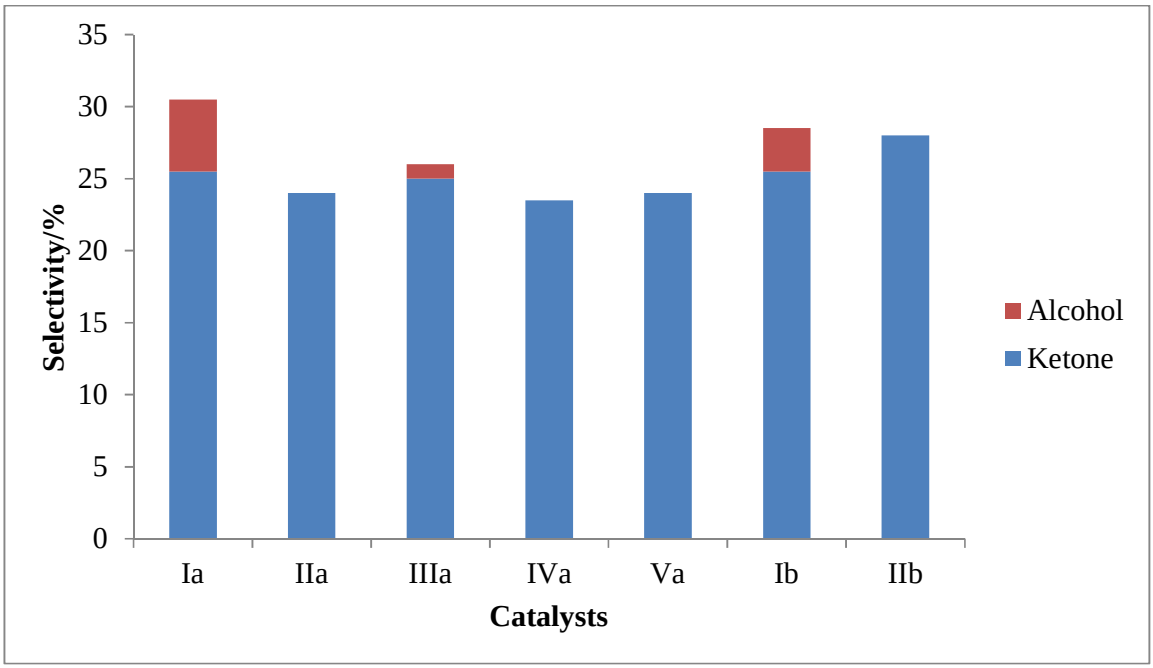

Figure 4.9: The selectivity to C(3) products for catalysts **Ia-IIb**

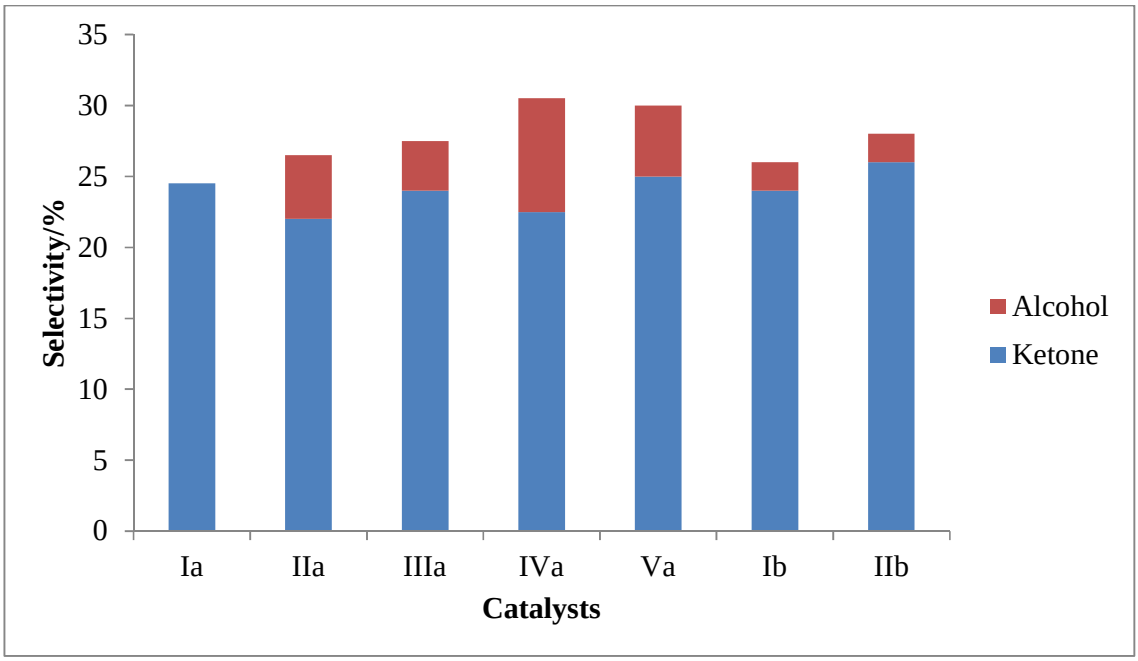

Figure 4.10: The selectivity to C(4) products for catalysts **Ia-IIb**.

The selectivity to the C(4) products (Fig. 4.10) revealed that ketones were the dominant products. Catalyst **IVa** displayed the highest conversion to 4-octanol (8%), followed by **Va**

(5%) and **IIa** (4.5%), with **Ib** and **IIb** exhibiting the lowest selectivity (2%). No conversion to the alcohol was observed for **Ia**.

Table 4.3 presents data on the regioselectivity parameter C(1):C(2):C(3):C(4) with respect to the reactivity of the hydrogen atoms at carbon positions 1, 2, 3 and 4 on the hydrocarbon chain which were normalised by accounting for the total number of hydrogens at each carbon position.

Regarding alcohol production, it is observed that **IIIa** (Entry 3) showed the highest alcohol selectivity at C(1), C(2) and C(4) compared to the other catalysts, while **Ia** (Entry 1) was the most selective at C(3). Focusing on the production of ketones, overall a similar pattern is observed from **IIIa-IIb** (Entry 3-Entry 7) with C(2) being the dominant position of attack. However, **IIa** proved to be the most selective catalyst at this position. The total regioselectivity parameter for each catalyst revealed that the hydrogens at position C(2) are the most reactive, while those at position C(1) are the least reactive, consistent with literature observations.[7,9] From Entry 7, it is evident that **IIb** displayed the highest selectivity at positions C(2), C(3) and C(4) which accounted for the higher overall ketone production at these positions. The trends of these parameters are comparable to those reported in the literature[8-9] for systems with *t*-BuOOH as the oxidant.

Table 4.3: Regioselectivity parameter C(1):C(2):C(3):C(4) in the oxidation of *n*-octane using *t*-BuOOH.

Entry	Catalyst	Alcohol C(1):C(2):C(3):C(4)	Ketone C(2):C(3):C(4)	Total[a] C(1):C(2):C(3):C(4)
1	**Ia**	1:3.5:3.1:0	1.3:1:1	1:5.8:4.6:3.7
2	**IIa**	1:1.7:0:1.9	1.5:1.1:1	1:3.9:2.5:2.8
3	**IIIa**	2:3.6:1:3.6	1.4:1:1	1:5.6:3.9:4.2
4	**IVa**	1:2.5:0:5	1.4:1:1	1:4.7:3.2:4.1
5	**Va**	1:1.5:0:2.5	1.4:1:1	1:3.8:2.6:3.2
6	**Ib**	1:1.9:2.1:1.4	1.4:1.1:1	1:4.1:3.3:3.0
7	**IIb**	1:1:0:3.3	1.4:1.1:1	1:8.3:6.4:6.4

[a] The selectivity of all products were taken into account i.e. ketones, alcohols, aldehyde and octanoic acid.

Table 4.4 summarises the turnover numbers (TON) calculated for each catalyst. This value gives an indication of the efficiency of the catalytic system. Catalyst **Ib** portrayed the highest TON of 23 with **Va** displaying the lowest of 9.3, which implies that **Ib** was the most efficient catalyst producing the most amount of product per unit mole of catalyst. For systems based on Co as the reactive metal and *t*-BuOOH as the oxidant, TONs in the mid teens have been reported.[2] Other systems containing Os as the reactive metal have reported TONs as high as 7500.[15] From this information it can be understood that although the Co-based catalysts do show some promise, they are yet not as efficient as other metal catalysts for the oxidation of saturated hydrocarbons.

Table 4.4: The turnover numbers (TON) calculated for catalysts **Ia**-**IIb**.

Catalyst	TON[a]
Ia	12.0
IIa	15.13
IIIa	10.2
IVa	7.5
Va	9.3
Ib	23.0
IIb	16.5

[a] TON = Moles of product (mol)/moles of catalyst (mol)

Scheme 4.2 presents the proposed pathway followed by the Co-SNS-*t*-BuOOH system in the oxidation of saturated hydrocarbons (RH). Similar pathways are presented in the literature for systems involving *t*-BuOOH in oxidation reactions.[1,9,16]

In the initial step, the Co^{II}(SNS) catalyst reduces *t*-BuOOH to generate the *tert*-butoxyl radical *t*-BuO• (eq 1). In the process a hydroxo-Co^{III} species is formed which can react further with *t*-BuOOH to produce Co^{III}(SNS)(OOBu-*t*) and water (eq 2). The *tert*-butylperoxy radical *t*-BuOO• is generated upon decomposition of Co^{III}(SNS)(OOBu-*t*) (eq 3) which can decompose further to yield the more reactive *t*-BuO• radical and oxygen (eq 4).[16] This radical then abstracts a hydrogen atom from the alkane to produce alkyl radicals R• (eq 5). The formation of peroxo radicals ROO• occurs upon reaction of R• with O_2 (eq 6), which can then lead to the production of the alkyl hydroperoxide ROOH (eq 7). Reaction of ROOH

with Co^{II}(SNS) can produce the organooxyl RO• radical (eq 8) which is able to abstract a hydrogen atom from the alkane to give rise to the alcohol and further alkyl radicals R• (eq 9). The peroxo radical ROO• can either decompose to form the alcohol and ketone (eq 10) or it can also undergo the mixed bimolecular Russell termination to produce more of the ketone and *t*-BuOH (eq 11), thus increasing the selectivity to the ketone.[9] Furthermore, secondary oxidation of the alcohol catalysed by Co^{II}(SNS) can lead to increased production of the ketone (eq 12).

$Co^{II}(SNS) + t\text{-BuOOH} \longrightarrow Co^{III}(SNS)(OH) + t\text{-BuO}\bullet$ **1**

$Co^{III}(SNS)(OH) + t\text{-BuOOH} \longrightarrow Co^{III}(SNS)(OOBu\text{-}t) + H_2O$ **2**

$Co^{III}(SNS)(OOBu\text{-}t) \longrightarrow Co^{III}(SNS) + t\text{-BuOO}\bullet$ **3**

$t\text{-BuOO}\bullet \longrightarrow t\text{-BuO}\bullet + \frac{1}{2} O_2$ **4**

$t\text{-BuO}\bullet + RH \longrightarrow R\bullet + t\text{-BuOH}$ **5**

$R\bullet + O_2 \longrightarrow ROO\bullet$ **6**

$ROO\bullet + RH \longrightarrow ROOH + R\bullet$ **7**

$Co^{II}(SNS) + ROOH \longrightarrow Co^{III}(SNS)(OH) + RO\bullet$ **8**

$RO\bullet + RH \longrightarrow ROH + R\bullet$ **9**

$2ROO\bullet \longrightarrow ROH + R_{\text{-H}}=O + O_2$ **10**

$ROO\bullet + t\text{-BuOO}\bullet \longrightarrow R_{\text{-H}}=O + t\text{-BuOH} + O_2$ **11**

$ROH + t\text{-BuOOH} \xrightarrow{Co^{II}(SNS)} R_{\text{-H}}=O$ **12**

Scheme 4.2: The proposed pathways followed in the oxidation of saturated hydrocarbons (RH) by a Co-SNS-*t*-BuOOH system in this study.

4.5 Summary and conclusions

The oxidation of *n*-octane using the prepared Co catalysts **Ia-IIb** was studied using two different oxidants: H_2O_2 and *t*-BuOOH. There was no substantial conversion observed in the system with H_2O_2, which proved to be an inefficient oxidant based on this study. The optimum reaction conditions were found to be: temperature of 80 °C, reaction time of 24 and 48 hours for the amine- and pyridine-based catalysts respectively, as well as a substrate to oxidant mole ratio of 1:20.

The dominant products were the ketones, with **IIb** showing the highest selectivity to the ketone products (ca. 90%) and consequently the lowest selectivity (4%) to the alcohols. The catalyst displaying the highest selectivity of ca. 15% to the alcohols was **IVa**, which offered more control over the selectivity due to the bulky cyclohexyl groups. In addition it was found that octanal and octanoic acid were products of over oxidation of 1-octanol and that the ketones were also formed from the secondary oxidation of the corresponding alcohols.

The carbon position C(2) was the most reactive as observed by the regioselectivity parameters and **IIb** exhibited the highest selectivity at C(2), C(3) and C(4). Overall the most efficient catalyst in terms of activity was **Ib**, with the highest total conversion of 23% and a TON of 23. From the pyridine-based catalysts, **Ia** was the most active with a total conversion of 12% and **IVa** was the least efficient catalyst overall displaying a conversion of 7% and the lowest TON of 7.5.

References

(1) (a) Chavez, F. A.; Mascharak, P. K. *Accounts of Chemical Research* **2000**, *33*, 539. (b) Chavez, F. A.; Nguyen, C. V.; Olmstead, M. M.; Mascharak, P. K. *Inorganic Chemistry* **1996**, *35*, 6282.

(2) Pozzi, G.; Cavazzini, M.; Quici, S.; Fontana, S. *Tetrahedron Letters* **1997**, *38*, 7605.

(3) Shul'pin, G. B. *C.R. Chimie* **2003**, *6*, 163.

(4) Costas, M.; Chen, K.; Que Jr., L. *Coordination Chemistry Reviews* **2000**, *200-202*, 517.

(5) Goldman, A. S.; Goldberg, K. I. In *Activation and Functionalization of C- H Bonds*; American Chemical Society, 2004; Vol. 885.

(6) Shilov, A. E.; Shul'pin, G. B. *Chemical Reviews* **1997**, *97*, 2879.

(7) Labinger, J. A.; Bercaw, J. E. *Nature* **2002**, *417*, 507.

(8) Shul'pina, L. S.; Kirillova, M. V.; Pombeiro, A. J. L.; Shul'pin, G. B. *Tetrahedron* **2009**, *65*, 2424.

(9) Mac Leod, T. C. O.; Kirillova, M. V.; Pombeiro, A. J. L.; Schiavon, M. A.; Assis, M. D. *Applied Catalysis A: General* **2010**, *372*, 191.

(10) Shul'pin, G. B.; Shilov, A. E.; Süss-Fink, G. *Tetraheron Letters* **2001**, *42*, 7253.

(11) Shul'pin, G. B.; Golfeto, C. C.; Süss-Fink, G.; Shul'pina, L. S.; Mandelli, D. *Tetrahedron Letters* **2005**, *46*, 4563.

(12) Mirkhani, V.; Moghadam, M.; Tangestaninejad, S.; Mohammadpoor-Baltork, I.; Rasouli, N. *Catalysis Communications* **2008**, *9*, 2411.

(13) Shul'pin, G. B.; Süss-Fink, G.; Shul'pina, L. S. *Journal of Molecular Catalysis A: Chemical* **2001**, *170*, 17.

(14) Cele, M. N., Master of Science thesis, University of KwaZulu-Natal, 2010.

(15) Yiu, S.; Man, W.; Lau, T. *Journal of the American Chemical Society* **2008**, *130*, 10821.

(16) Förster, S.; Rieker, A.; Maruyama, K.; Murata, K.; Nishinaga, A. *The Journal of Organic Chemistry* **1996**, *61*, 3320.

CHAPTER FIVE

General Conclusion

The preparation of a series of pincer-type SNS ligands has been achieved with two different backbones investigated: a constrained six membered pyridine ring and a linear straight chained amine. All ligands were characterised using NMR, IR and MS and the successful complexation of seven out of the eight ligands to Co was achieved. The Co complexes were characterised by IR, elemental analysis and melting point, which confirmed that the SNS ligands coordinated to the metal centre and the complexes were of high purity. The crystal structures of Co(SNS-mepy)Cl_2 (**Ia**), Co(SNS-etpy)Cl_2 (**IIa**) and Co(SNS-butpy)Cl_2 (**IIIa**) were determined confirming that the SNS ligands were terdentate and coordinated to the metal centre via the N- and S-donor atoms.

The Co complexes (**Ia-IIb**) were tested for the activation and oxidative functionalisation of *n*-octane as the substrate. In this study, two different oxidant sources were investigated: H_2O_2 and *t*-BuOOH. The results showed that *t*-BuOOH was the more efficient oxidant and no catalytic activity was observed with H_2O_2 as oxidant. The reaction between the respective catalysts and *n*-octane in the presence of *t*-BuOOH produced a mixture of C-8 alcohols and carbonyl compounds which were oxygenated at positions 1, 2, 3 and 4 of the C-8 carbon chain.

When the activity of the catalysts in each series were compared, it was found that **Ia** was the most active catalyst in the pyridine-based series giving the highest total conversion of 12%, while **Ib** was the most active catalyst in the amine-based series showing the highest total conversion of 23%. Overall, the amine-based catalysts proved to be the most efficient catalysts, as they exhibited significantly higher conversions as compared to the pyridine-based catalysts.

According to the selectivity profile for each catalyst, the ketone products were the most dominant, with 2-octanone being formed in larger quantities than the other ketones. The regioselectivity parameters also revealed that C(2) was the most prominent position of attack on the hydrocarbon chain for all the catalysts studied. It was also discovered that as the

bulkiness of the substituents attached to the S-donor atoms increased, there was more control over the selectivity to the alcohol products, as catalyst **IVa** ($Co(SNS\text{-}cypy)Cl_2$) exhibited the highest selectivity of 15% to the alcohols.

Finally, it can be concluded that the main goals of this study were achieved because the catalysts were successfully synthesised, characterised and tested for their activity in paraffin oxidation. Indeed there was considerable activity observed with all prepared catalysts, however from the results obtained, the amine-based catalysts together with *t*-BuOOH were the most efficient catalytic systems in this work.

Supporting information

Supporting information includes data on ^{1}H, ^{13}C and ^{13}C DEPT 135 NMR, IR, single crystal X-ray crystallography and catalytic results, which are provided as individual pdf documents on the compact disc accompanying this thesis. The data is presented in the same order corresponding to the chapter arrangement of the thesis report. This is to ensure that the total volume of the printed text is manageable and within the acceptable limit. Readers are encouraged to access the raw data for further information.